Article

Adenosine signalling drives antidepressant actions of ketamine and ECT

https://doi.org/10.1038/s41586-025-09755-9

Received: 27 January 2025

Accepted: 14 October 2025

Published online: 5 November 2025

Open access

Check for updates

Chenyu Yue[1,2,3,4,5,12], Na Wang[2,6,12], Haojiang Zhai[7,8], Zhengwei Yuan[1,2,4], Yuting Cui[1,2,4], Jing Quan[1,2,4], Yu Zhou[1,2,4], Xiaofeng Fan[2], Hongshuang Wang[7], Zhaofa Wu[9], Huijie Mi[1,2], Wooping Ge[1,2], Yulong Li[10,11], Xiaohui Wang[7,8]✉ & Minmin Luo[1,2,3,4,11]✉

Ketamine and electroconvulsive therapy (ECT) achieve rapid remission in treatment-resistant depression. However, their mechanisms of action—the understanding of which is essential for refining therapeutic precision—remain unclear[1–3]. Here, using mouse models, we identify adenosine signalling as a central pathway that underlies the antidepressant effects of these interventions. Results from genetically encoded adenosine sensor experiments and real-time optical recordings reveal that both therapies induce strong adenosine surges in key mood-regulatory regions, including the medial prefrontal cortex and the hippocampus. Genetic or pharmacological disruption of A_1 and A_{2A} adenosine receptors abolishes their therapeutic effects, which establishes the essential role of adenosine signalling in antidepressant efficacy. Notably, adenosine signalling specifically in the medial prefrontal cortex drives antidepressant actions. Ketamine increases adenosine by modulating cellular metabolism to increase intracellular adenosine levels without causing neuronal hyperactivity. Leveraging this mechanism, we develop ketamine derivatives that enhance adenosine signalling and exhibit improved antidepressant efficacy with reduced side effects at therapeutic doses. Furthermore, acute intermittent hypoxia, a non-pharmacological intervention involving controlled reductions in oxygen levels, increases brain adenosine levels and produces antidepressant effects, paralleling the actions of ketamine and ECT. Our findings establish adenosine as a pivotal mediator of rapid-acting antidepressants and a tractable target for scalable, noninvasive therapeutics in major depressive disorder.

A single subanaesthetic dose of ketamine induces rapid, robust and enduring antidepressant effects that often manifest within hours and persist for days[1,2]. This efficacy has galvanized efforts to uncover the molecular and cellular mechanisms that underlie its therapeutic action, with the goal of developing safer and more effective treatments[4–11]. Originally identified as an NMDA receptor (NMDAR) antagonist[12], ketamine is now understood to influence a network of neuromodulators. Ketamine alters neuronal activity and promotes synaptic plasticity in brain regions implicated in major depressive disorder (MDD), such as the medial prefrontal cortex (mPFC) and the hippocampus[9,13,14]. Electroconvulsive therapy (ECT), another rapid-acting antidepressant intervention, has also been shown to engage multiple neuromodulators in the brain. The underlying mechanisms of ECT also remain incompletely understood[3,15].

To identify the neuromodulator that underlies these therapies, the following key criteria should be met: both ketamine and ECT should change neuromodulator levels in the brain, and activation or inhibition of the associated signalling pathways should either replicate or abolish antidepressant effects. Moreover, insights into these mechanisms should guide the development of new therapeutic strategies. Although numerous candidates have been proposed as the key neuromodulator[9,13,14], many do not fully satisfy these stringent criteria, which underscores the need for continued exploration to identify a central player.

Emerging evidence suggests that adenosine, a purine nucleoside with high-affinity A_1 (encoded by *Adora1*) and A_{2A} (encoded by *Adora2a*) receptors[16,17], is a promising but underexplored candidate. Adenosine regulates neuronal excitability, synaptic plasticity and inflammatory responses[16], all of which are implicated in MDD[18]. Dysregulated adenosine metabolism has been linked to depressive symptoms[19], and interventions that enhance adenosine signalling, such as sleep deprivation[20,21] and ketogenic diets[22], have shown antidepressant-like effects in

[1]Beijing Institute for Brain Research, Chinese Academy of Medical Sciences and Peking Union Medical College, Beijing, China. [2]Chinese Institute for Brain Research, Beijing, China. [3]National Institute of Biological Sciences, Beijing, China. [4]Research Unit of Medical Neurobiology, Chinese Academy of Medical Sciences, Beijing, China. [5]Peking University–Tsinghua University–NIBS Joint Graduate Program, NIBS, Beijing, China. [6]School of Basic Medical Sciences, Capital Medical University, Beijing, China. [7]Laboratory of Chemical Biology, Changchun Institute of Applied Chemistry, Chinese Academy of Sciences, Changchun, China. [8]Department of Applied Chemistry and Engineering, University of Science and Technology of China, Hefei, China. [9]Laboratory of Integrative Physiology, Institute of Genetics and Developmental Biology, Chinese Academy of Sciences, University of Chinese Academy of Sciences, Beijing, China. [10]State Key Laboratory of Membrane Biology, School of Life Sciences, Peking University, Beijing, China. [11]New Cornerstone Science Laboratory, Shenzhen, China. [12]These authors contributed equally: Chenyu Yue, Na Wang. ✉e-mail: xiaohui.wang@ciac.ac.cn; luominmin@cibr.ac.cn

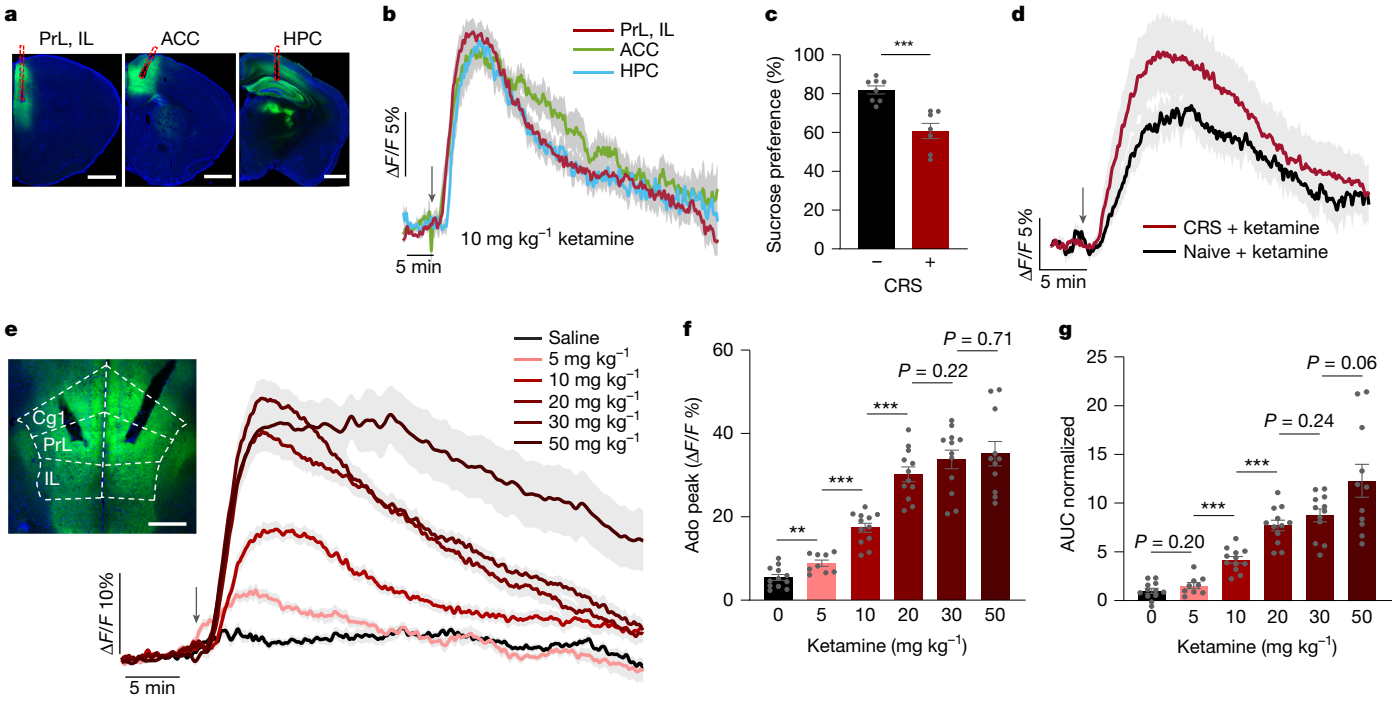

Fig. 1 | Ketamine induces adenosine surges in the brain. a, Representative images of $GRAB_{Ado1.0}$ expression (green) in the ACC, the HPC and the PrL and IL of the mPFC. Red dashed lines indicate tracks of the optical fibre. Scale bars, 1 mm. **b**, Time course of extracellular adenosine levels in the mPFC (red; $n = 12$ mice), ACC (green; $n = 8$ mice) and HPC (blue; $n = 8$ mice) after ketamine administration (10 mg kg^{-1}, i.p. injection; arrow). **c**,**d**, Sucrose preference in mice subjected to CRS versus naive mice (**c**) and the corresponding time course of extracellular adenosine levels in the mPFC after ketamine administration (10 mg kg^{-1}, i.p. injection) (**d**). **e**–**g**, Dose–response effects of ketamine on extracellular adenosine levels in the mPFC. **e**, Time course after ketamine injections (5, 10, 20, 30 or 50 mg kg^{-1}, i.p. injection) and saline control. Image shows the recording site. Cg1, cingulate cortex 1, which is part of the ACC. Scale bar, 500 µm. **f**,**g**, Adenosine (Ado) peak levels (**f**) and area under the curve (AUC; normalized to saline) (**g**) after drug administration. Data are the mean ± s.e.m. (shading in **b**, **d** and **e**; error bars in **c**, **f** and **g**). Statistics: two-tailed unpaired *t*-tests (**c**,**f**,**g**). $^{**}P < 0.01$, $^{***}P < 0.001$. See Supplementary Table 1 for detailed statistics.

humans and animal models. Despite the therapeutic potential of ketamine and ECT, studying the role of adenosine in these treatments has been technically challenging owing to the transient and dynamic nature of its signalling and its brain-region-specific and receptor-specific actions[16,23,24]. Notably, although adenosine generally exhibits neuroprotective and antidepressant properties, chronic A_{2A} receptor activation in certain brain regions may counteract these benefits[19,25], which highlights the complexity of its spatiotemporal regulation.

Here we use genetically encoded adenosine sensors to reveal rapid adenosine surges in mood-regulatory circuits after ketamine administration or ECT. Notably, systemic or specific depletion or blockade of A_1 and A_{2A} receptors in the mPFC abolishes the antidepressant efficacy of these therapies. Moreover, the activation of these two receptors recapitulates therapeutic effects, thereby demonstrating the pivotal role of adenosine. Building on these insights, we identify ketamine derivatives that potentiate adenosine signalling to produce enhanced antidepressant efficacy and reduced side effects. We further demonstrate that acute intermittent hypoxia (aIH), a noninvasive method that involves controlled oxygen reduction, is a potent adenosine-dependent antidepressant strategy. These findings establish adenosine signalling as the central mechanism that unifies the actions of ketamine and ECT and open new therapeutic avenues for MDD.

Ketamine triggers brain adenosine surges

We first investigated the effects of ketamine on extracellular adenosine dynamics. To that end, we used the GPCR-based adenosine probe $GRAB_{Ado1.0}$ with multichannel fibre photometry to enable real-time monitoring of adenosine levels in the mouse brain (Extended Data Fig. 1a). We first validated the fidelity of this sensor in vivo. Acute hypoxia, a potent physiological stimulus for adenosine release[26], induced a rapid increase in the $GRAB_{Ado1.0}$ signal. By contrast, a functionally inactive mutant sensor ($GRAB_{Ado1.0\text{-}mut}$) did not produce any effects. This result confirms the specificity of $GRAB_{Ado1.0}$ for detecting changes in extracellular adenosine levels (Extended Data Fig. 1b).

Systemic administration of a subanaesthetic, antidepressant dose of ketamine (10 mg kg^{-1}, intraperitoneal (i.p.) injection) caused a rapid and sustained increase in extracellular adenosine in the mPFC—an area comprising the prelimbic (PrL), infralimbic (IL) and anterior cingulate (ACC) cortices—and in the hippocampus (HPC), but not in the nucleus accumbens (NAc) (Fig. 1a,b and Extended Data Fig. 1c). The adenosine surge featured peak amplitudes of about 15% change in fluorescence ($\Delta F/F$), onset times of 100–150 s after injection, peak times of about 500 s and decay time constants of 500–600 s after the peak (Extended Data Fig. 1d–h). Two-photon imaging confirmed that this release was spatially diffuse (Extended Data Fig. 1i–k). Notably, ketamine induced a similar increase in adenosine levels in mice subjected to chronic restraint stress (CRS) (a mouse model of depression). These results demonstrate that this neurochemical response is reliable across physiological and pathological states (Fig. 1c,d and Extended Data Fig. 1l).

The ketamine-induced adenosine increase in the mPFC was dose-dependent. A low dose (5 mg kg^{-1}) produced a modest signal, whereas the response amplitude and duration increased substantially at 10 and 20 mg kg^{-1}. Higher doses (30 and 50 mg kg^{-1}) did not further augment the peak amplitude but prolonged the signal decay time (Fig. 1e–g and Extended Data Fig. 1m,n). This effect reflected endogenous adenosine release, as ketamine did not directly activate the $GRAB_{Ado1.0}$ sensor (Extended Data Fig. 1o,p). The kinetics of the ketamine response were distinct from those of acute hypoxia, inducing a signal with a smaller

peak amplitude (around 35% for high ketamine doses compared with about 60% $\Delta F/F$ for hypoxia) but a markedly slower decay (>500 s compared with about 50 s) (Fig. 1e and Extended Data Fig. 1b). These results demonstrate that the modulation of adenosine by ketamine operates within the dynamic range of the sensor and aligns with its therapeutically relevant subanaesthetic doses.

We next investigated whether the adenosine surge is triggered by ketamine itself or by its metabolites (Extended Data Fig. 2a). Systemic administration of two primary metabolites, norketamine (NK) and (2*R*,6*R*)-HNK[10], at an equivalent dose (10 mg kg^{-1}, i.p. injection) did not trigger a detectable adenosine response in the mPFC (Extended Data Fig. 2b,c). To corroborate this finding, we pharmacologically inhibited key enzymes responsible for ketamine metabolism in vivo[27]. Pretreatment with the CYP3A4 inhibitors ketoconazole or ritonavir significantly potentiated the amplitude and duration of the ketamine-induced adenosine signal (Extended Data Fig. 2d–g). By contrast, inhibition of CYP2B6 with ticlopidine had no effect (Extended Data Fig. 2h,i). Because the inhibitors alone did not alter baseline adenosine levels (Extended Data Fig. 2j–l), these results suggest that the parent ketamine molecule is directly responsible for triggering adenosine release, the magnitude of which is regulated by CYP3A4-mediated metabolism.

Adenosine drives the action of ketamine

To determine whether adenosine signalling is required for the antidepressant action of ketamine, we first confirmed its efficacy in wild-type (WT) mice subjected to CRS and then to forced swim tests (FSTs) or sucrose preference test (SPTs), which are behavioural assays for despair and anhedonia, respectively (Fig. 2a). Given the established roles of adenosine A_1 and A_{2A} receptors in central adenosine signalling[24,28,29], we evaluated ketamine in *Adora1*$^{-/-}$ and *Adora2a*$^{-/-}$ mice (Supplementary Fig. 1). The antidepressant effects of ketamine, assessed at both 1 h (acute) and 24 h (sustained) after administration, were abolished in both knockout mouse lines (Fig. 2b–e).

The loss of therapeutic action in the knockout mice was not attributable to motor confounds and occurred despite the preservation of ketamine-induced hyperlocomotion, which was comparable between WT and mutant mice (Extended Data Fig. 3a–c). These results therefore dissociate the antidepressant properties of the drug from its psychostimulant side effects. We also confirmed that the behavioural deficits in knockout mice resulted from receptor absence rather than a developmental impairment in adenosine release. That is, the ketamine-induced adenosine surge remained intact in both *Adora1*$^{-/-}$ and *Adora2a*$^{-/-}$ mice (Extended Data Fig. 3d).

Complementing these genetic data, acute pharmacological blockade in WT mice subjected to CRS revealed a pivotal role for both receptors (Extended Data Fig. 3e–i). Pretreatment with a selective A_1 receptor antagonist completely abolished the antidepressant-like effects of ketamine in FSTs, whereas A_{2A} receptor blockade produced a reduced attenuation 1 h after ketamine administration (Extended Data Fig. 3f,h). This result confirms the necessity of adenosine receptor activity for reducing behavioural despair[30,31]. A similar dependency was observed for anhedonia, whereby A_1 and, to a lesser extent, A_{2A} receptor antagonism prevented ketamine from reversing deficits in sucrose preference (Extended Data Fig. 3g,i). This requirement for adenosine receptor signalling was not specific to the CRS model, as inhibition of both receptors also blunted the efficacy of ketamine in a mouse model of depression induced by lipopolysaccharide (LPS)[32] (Extended Data Fig. 3j).

Collectively, these converging data—derived from complementary genetic and pharmacological approaches in both stress-induced and inflammation-induced depression models—establish that the efficacy of ketamine in reversing core depressive-like behaviours, including anhedonia and behavioural despair, depends on adenosine signalling.

mPFC adenosine signalling is crucial

We asked whether adenosine signalling is sufficient to induce antidepressant effects. Intracerebroventricular injection of adenosine or systemic delivery of selective agonists of the A_1 receptor (N^6-cyclohexyladenosine (CHA)) and the A_{2A} receptor (CGS21680) replicated the immediate therapeutic effects of ketamine in mice subjected to CRS (Extended Data Fig. 4a–c). Notably, 24 h after administration, only CHA—but not CGS21680—retained efficacy in behavioural assays (Extended Data Fig. 4d,e). This lasting therapeutic action occurred despite the agonist being cleared from the brain by 24 h (Extended Data Fig. 4f), which indicated that transient A_1 receptor activation triggers a durable antidepressant state, whereas A_{2A} receptor signalling contributes primarily to acute effects.

To test whether localized adenosine signalling is sufficient to produce an antidepressant effect, we focused on the mPFC, a key region implicated in both mood regulation and the therapeutic action of ketamine. Direct stereotaxic infusion of adenosine into the mPFC produced a robust antidepressant response (Extended Data Fig. 5a–c). To corroborate this finding with a more physiologically relevant approach, we used optogenetics to stimulate astrocytes expressing cOpn5, which triggers localized, adenosine release that is mediated by CD73 (encoded by *Nt5e*)[33] (Fig. 2f). This light-induced adenosine production, specifically in the mPFC, was also sufficient to alleviate depressive-like behaviours in WT mice, an effect that was absent in *Nt5e*$^{-/-}$ knockout mice (Fig. 2g–i and Extended Data Fig. 5d). The behavioural rescue was associated with changes in a key molecular pathway, as ketamine-induced upregulation of brain-derived neurotrophic factor (BDNF)—a canonical downstream effector[34,35]—was prevented in *Adora1*$^{-/-}$ and *Adora2a*$^{-/-}$ mice, in which these receptors are globally knocked out (Extended Data Fig. 5e and Supplementary Fig. 2a). In support of the circuit-specificity of this mechanism, neither local adenosine infusion nor optogenetic stimulation in the dorsal hippocampus produced any antidepressant actions (Extended Data Fig. 5f–j).

Having established that adenosine signalling in the mPFC is sufficient, we next investigated whether this circuit is also necessary for the therapeutic effects of systemic ketamine. To that end, we used the adeno-associated virus (AAV)-mediated CRISPR–Cas9 approach and delivered single-guide RNAs (sgRNAs) into the mPFC of adult mice to genetically deplete A_1 and A_{2A} receptor expression (Extended Data Fig. 5k and Supplementary Fig. 1). This circuit-restricted knockout also abolished the antidepressant behavioural effects of systemic ketamine in both the FSTs and SPTs (Extended Data Fig. 5l,m). Together, these results establish that adenosine signalling in the mPFC is a critical node that mediates rapid antidepressant efficacy.

Metabolic basis for adenosine efflux

To investigate how ketamine increases extracellular adenosine concentrations in the brain, we first considered whether adenosine is generated through the hydrolysis of extracellular adenine nucleotides by CD73 (ref. 36) (Extended Data Fig. 6a). Using $GRAB_{ATP1.0}$, a sensor capable of detecting both ATP and ADP, we monitored purine dynamics in the mPFC. Ketamine administration did not increase extracellular ATP or ADP levels; instead, it caused a modest reduction (Extended Data Fig. 6b–d). Furthermore, genetic depletion of CD73 did not have an effect on ketamine-induced adenosine signals (Extended Data Fig. 6e–g and Supplementary Fig. 2b). These findings exclude extracellular nucleotide hydrolysis as the primary source of ketamine-induced increases in extracellular adenosine levels.

An alternative source of extracellular adenosine originates from the activity of the equilibrative nucleoside transporters ENT1 and ENT2 (ENT1/2), which regulate the balance between intracellular and extracellular adenosine levels[23,36] (Fig. 3a). We proposed that blocking the activity of ENT1/2 would increase ketamine-induced adenosine signals

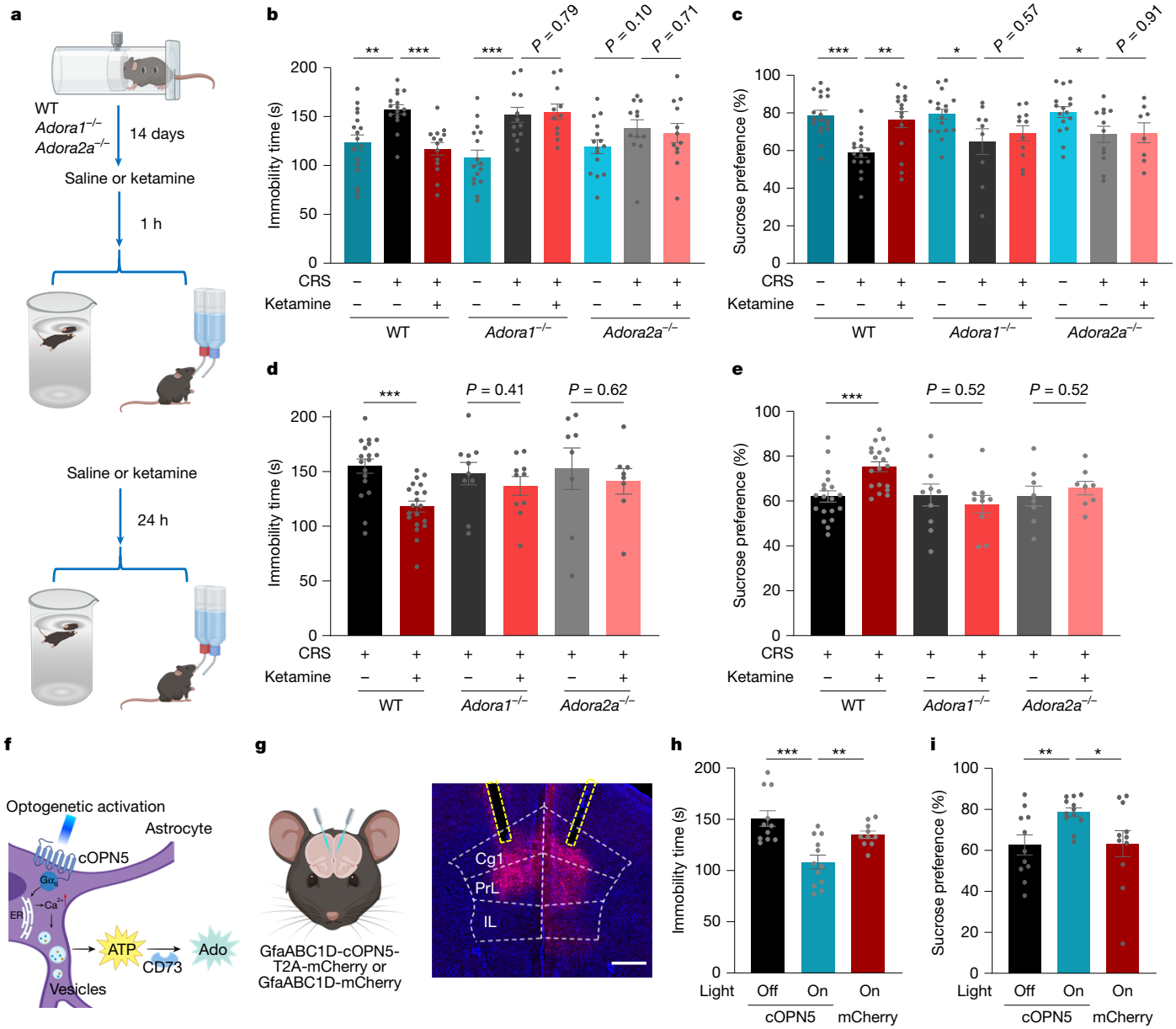

Fig. 2 | Adenosine signalling drives the antidepressant action of ketamine. a, Experimental timeline for assessing the antidepressant action of ketamine at 1 and 24 h in WT, *Adora1*$^{-/-}$ and *Adora2a*$^{-/-}$ mice subjected to CRS. **b**–**e**, FSTs (**b**,**d**) and SPTs (**c**,**e**) were performed after CRS in WT, *Adora1*$^{-/-}$ and *Adora2a*$^{-/-}$ mice 1 h (**b**,**c**) or 24 h (**d**,**e**) after ketamine administration (10 mg kg^{-1}, i.p. injection). **f**–**i**, Optogenetic release of adenosine in the mPFC produces rapid antidepressant-like effects. **f**, Schematic of optogenetic astrocyte activation that leads to adenosine production via ectonucleotidase activity (for example, CD73). ER, endoplasmic reticulum. **g**, Schematic and representative image of optogenetic activation. Scale bar, 500 µm. **h**,**i**, Immobility times in FSTs (**h**) and sucrose preference in SPTs (**i**) were measured 1 h after optogenetic activation in mice expressing the light-sensitive opsin cOpn5 or a mCherry control in the mPFC and subjected to CRS. Data are the mean ± s.e.m. (error bars in **b**–**e**,**h**,**i**). Statistics: two-tailed unpaired *t*-tests (**b**–**e**,**h**,**i**). *$P < 0.05$, **$P < 0.01$, ***$P < 0.001$. See Supplementary Table 1 for detailed statistics. The schematics in **a**, **f** and **g** were created using BioRender (https://www.biorender.com).

if adenosine was produced outside cells, whereas the opposite would occur if adenosine was produced inside cells and then released through ENT1/2 activity. To test this hypothesis, we first inhibited ENT1/2 using intracranial administration of dipyridamole, an ENT1/2 inhibitor. This treatment significantly attenuated ketamine-induced adenosine signals (Fig. 3b,c), whereas dipyridamole alone did not cause rapid increases in extracellular adenosine levels (Extended Data Fig. 6h,i). These results suggest that ketamine disrupts the intracellular–extracellular adenosine equilibrium, probably by increasing intracellular adenosine and subsequently transporter-mediated efflux.

Intracellular adenosine accumulation is closely associated with shifts in cellular metabolic activity, particularly reductions in the ATP/ADP ratio[23,37,38]. To assess whether ketamine modulates ATP/ADP dynamics in neurons and glia, we used PercevalHR—a genetically encoded sensor of the intracellular ATP/ADP ratio—in the mPFC[37]. This method enabled us to track metabolic changes in excitatory neurons, inhibitory neurons and astrocytes (Fig. 3d–f). Ketamine administration rapidly decreased the ATP/ADP ratio across all cell types, with the largest reduction in excitatory CaMKII-expressing pyramidal neurons (Fig. 3d). GABAergic neurons showed an initial reduction followed by a rebound, whereas astrocytes exhibited a sustained decrease (Fig. 3e,f). Analysis of $GRAB_{Ado1.0}$ and PercevalHR temporal response profiles revealed that reduction in the intracellular ATP/ADP ratio preceded the extracellular adenosine surge (Extended

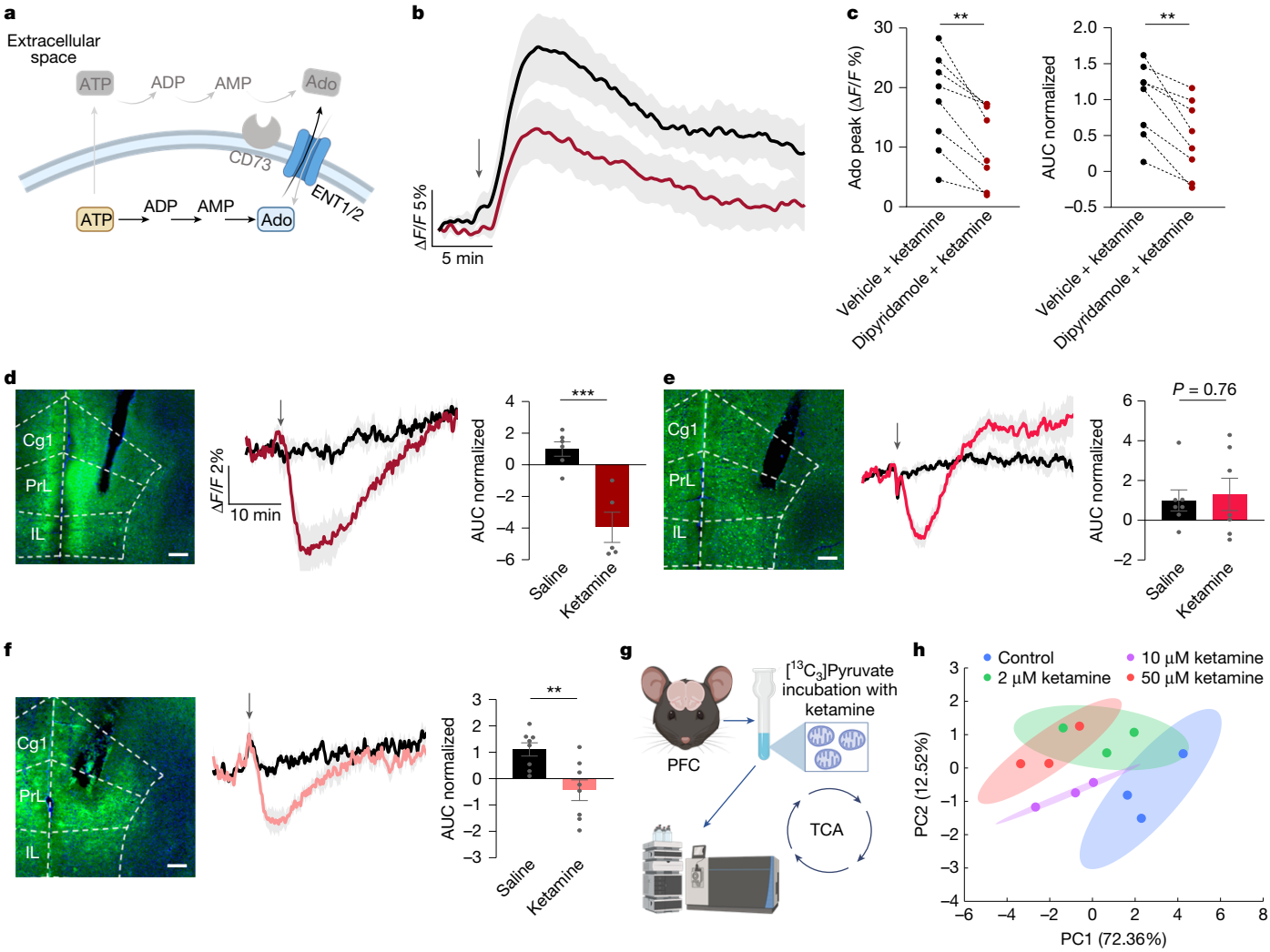

Fig. 3 | Ketamine modulates cellular metabolism and promotes adenosine efflux via ENT1/2. a, Schematic of intracellular adenosine generation and its efflux through ENT1/2. **b**,**c**, Inhibition of ENT1/2 blocks ketamine-induced adenosine release. **b**, Time course of extracellular adenosine in the mPFC after ketamine administration with or without pretreatment with the ENT1/2 inhibitor dipyridamole (1 μg, intracerebroventricular injection). **c**, Quantification of peak adenosine and AUC (normalized to vehicle). **d**, Ketamine decreases the intracellular ATP/ADP ratio in mPFC excitatory neurons. Left, representative image of PercevalHR expression in CaMKII$^+$ neurons. Scale bar, 200 μm. Middle, time course of the ATP/ADP ratio after ketamine (10 mg kg^{-1}, i.p. injection) or saline treatment. Right, corresponding AUC (normalized to saline). **e**,**f**, Intracellular ATP/ADP ratios in mPFC GABAergic neurons (**e**) and astrocytes (**f**). Panels show representative images, time courses and saline-normalized AUCs as in **d**. **g**, Experimental workflow for mitochondrial isolation and subsequent metabolic flux analyses in the mouse prefrontal cortex. **h**, PCA of the metabolomic profiles, illustrating separation of the treatment groups along the first two principal components. Ellipses represent 95% confidence intervals calculated using the multivariate *t*-distribution. Data are the mean ± s.e.m. (shading in **b**, **d**–**f**; error bars in **c**–**f**). Statistics: two-tailed paired *t*-test (**c**) or two-tailed unpaired *t*-tests (**d**–**f**). $^{**}P < 0.01$, $^{***}P < 0.001$. See Supplementary Table 1 for detailed statistics. The schematics in **a** and **g** were created using BioRender (https://www.biorender.com).

Data Fig. 6p,q). This temporal sequence strongly supports the hypothesis that ketamine-induced metabolic alterations drive adenosine efflux, which then lead to the observed increase in extracellular adenosine levels.

Adenosine build-up in cells typically arises from increased cellular metabolic activity[23,37,38], which is often triggered by excessive excitability in neurons, as seen during epileptic states. To determine whether ketamine induces neuronal hyperactivity, we monitored intracellular Ca^{2+} dynamics using the Ca^{2+} indicator GCaMP8s expressed in mPFC neurons. In pyramidal neurons, ketamine significantly reduced Ca^{2+} signalling at a high dose (20 mg kg^{-1}) but not at the standard antidepressant dose (10 mg kg^{-1}) (Extended Data Fig. 6j–l). Moreover, GABAergic neurons exhibited a decrease in Ca^{2+} activity at the dose of 10 mg kg^{-1} (Extended Data Fig. 6m–o). Thus, ketamine induces adenosine signals by altering cellular metabolism and promoting transporter-mediated efflux while avoiding neuronal hyperactivity.

To determine whether ketamine directly targets mitochondria to modulate cellular metabolism, we performed metabolic flux analyses on purified brain mitochondria. By incubating isolated mitochondria from the mPFC with [$^{13}C_3$]pyruvate, we traced the entry and metabolism of this key substrate through the TCA cycle in the presence of ketamine (Fig. 3g and Extended Data Fig. 7a). At therapeutically relevant concentrations (≥2 μM)[39,40], ketamine exposure caused an accumulation of [^{13}C]pyruvate while dose-dependently suppressing the ^{13}C enrichment of downstream TCA cycle intermediates, including fumarate, malate and aspartate (Extended Data Fig. 7b,c). The metabolic changes were reflected in a global dose-dependent shift in the mitochondrial metabolome, as shown by principal component analysis (PCA) (Fig. 3h). This inhibitory effect on pyruvate utilization was consistent with a decrease in the ATP/ADP ratio. This result provides a mechanistic link between the action of ketamine at the mitochondrion and the observed surge in extracellular adenosine. Crucially, as these metabolic alterations

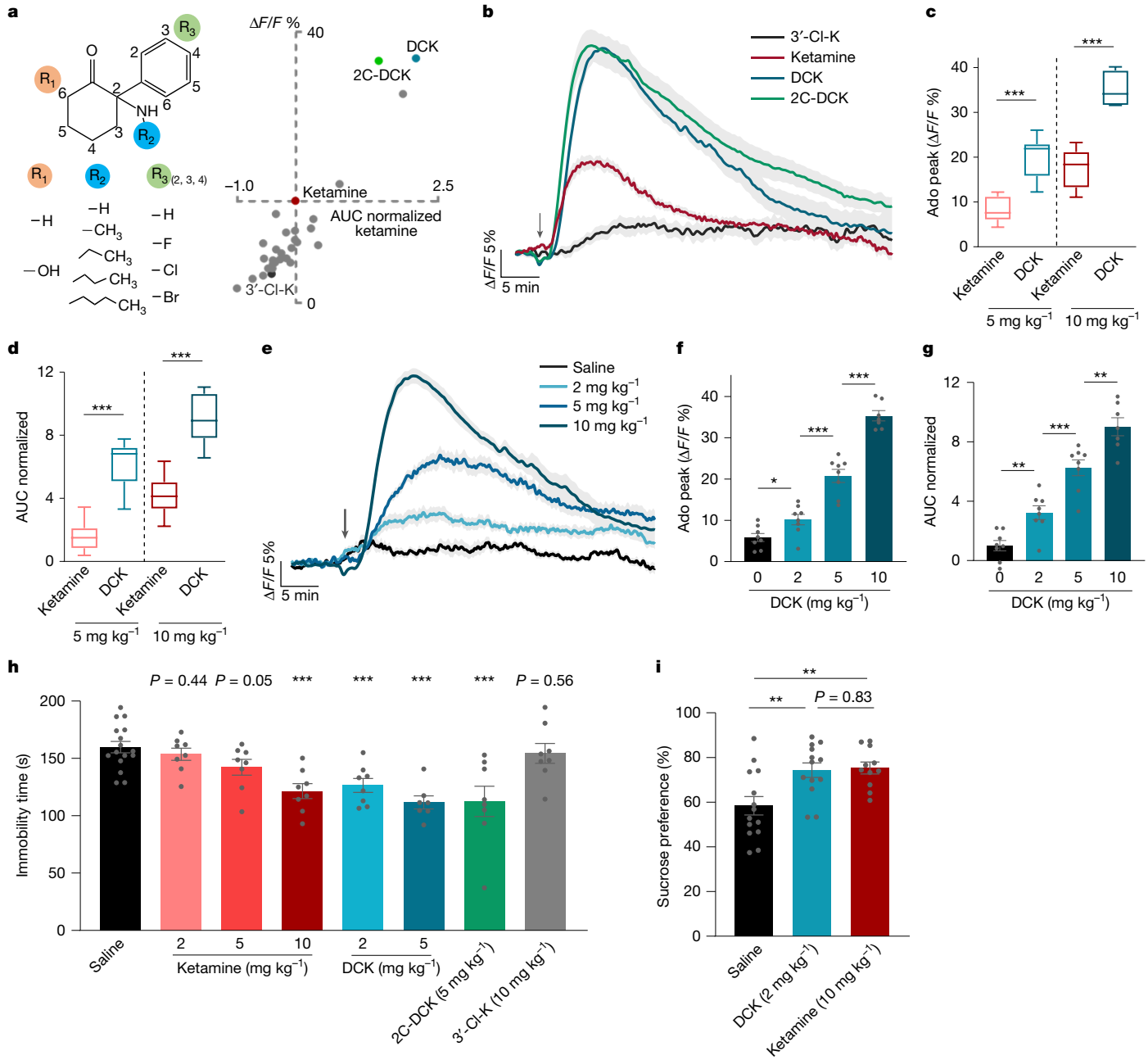

Fig. 4 | Adenosine-based screening identifies ketamine analogues with potent antidepressant-like effects. a, Left, schematic of the ketamine analogue synthesis strategy. Right, scatter plot of peak adenosine amplitude compared with the AUC from an in vivo screen of synthesized compounds (10 mg kg^{-1}, i.p. injection), normalized to ketamine responses. **b**, Time course of extracellular adenosine levels in the mPFC after administration of DCK ($n = 7$ mice), 2C-DCK ($n = 8$ mice), 3′-Cl-ketamine ($n = 6$ mice) or ketamine ($n = 13$ mice; 10 mg kg^{-1}, i.p. injection; arrow). **c**,**d**, Comparison of peak adenosine levels (**c**) and AUC (**d**; normalized to saline) for DCK versus ketamine at an equivalent dose. **e**–**g**, Dose–response of DCK on adenosine release in the mPFC. **e**, Time course following injections of DCK (2, 5 and 10 mg kg^{-1}, i.p. injection) or saline. **f**, Peak adenosine levels. **g**, AUC, normalized to saline. **h**,**i**, Rapid antidepressant-like effects of lead analogues. Immobility time in FSTs (**h**) and sucrose preference in SPTs (**i**) were measured in mice subjected to CRS 1 h after i.p. administration of ketamine, DCK, 2C-DCK or 3′-Cl-ketamine (3′-Cl-K). Data are the mean ± s.e.m. (shading in **b** and **e**; error bars in **c**, **d** and **f**–**i**). Box plots (**c**,**d**) show the median (centre line), first and third quartiles (box bounds), and 1.5× the interquartile range (whiskers). Statistics: two-tailed unpaired *t*-tests (**c**,**d**,**f**–**i**). $^{*}P < 0.05$, $^{**}P < 0.01$, $^{***}P < 0.001$. In **h**, significance is relative to the saline control. See Supplementary Table 1 for detailed statistics.

occur in an isolated organelle system that lacks NMDARs, our findings indicate that subanaesthetic ketamine may directly engage and reprogram mitochondrial function.

Ketamine-derived antidepressants

To identify new compounds with enhanced therapeutic profiles, we used a phenotypic drug discovery approach using adenosine dynamics in the mPFC as a functional biomarker. We synthesized and screened 31 ketamine-derived compounds by systematically modifying the chloro substituent (-Cl) on the aromatic ring, the methylamino group attached to the cyclohexanone ring and the sixth position of the cyclohexanone ring—a key site for hydroxylation during metabolism (Fig. 4a, Extended Data Fig. 8a and Supplementary Methods). By leveraging fibre photometry, we assessed the capacity of these compounds to enhance extracellular adenosine levels in the mPFC. Although most compounds

produced weak or no adenosine responses, dechlorinated derivatives, particularly deschloroketamine (DCK) and deschloro-*N*-ethyl-ketamine (2C-DCK), induced significantly stronger and longer-lasting adenosine surges than ketamine at the same doses of 5 and 10 mg kg^{-1} (Fig. 4b–d and Extended Data Fig. 8b), indicating their potential as improved therapeutic agents. Further dose mapping revealed that even at a low dose of 2 mg kg^{-1}, DCK significantly increased extracellular adenosine levels (Fig. 4e–g). This result highlights the strong adenosine-modulating properties of DCK and its potential efficacy at lower doses.

We investigated whether the strong adenosine signals induced by DCK and 2C-DCK translate to antidepressant efficacy. In FSTs of mice subjected to CRS, ketamine at 10 mg kg^{-1} significantly decreased immobility time, whereas 5 mg kg^{-1} showed marginal effects, and lower doses were ineffective. By contrast, DCK displayed substantial efficacy at substantially lower doses: 2 mg kg^{-1} significantly alleviated depressive behaviours, and 5 mg kg^{-1} produced even greater improvements (Fig. 4h). Similarly, in SPTs, 2 mg kg^{-1} DCK demonstrated antidepressant effects equivalent to 10 mg kg^{-1} ketamine (Fig. 4i). These results highlight the enhanced potency of DCK compared with ketamine. In parallel, 2C-DCK, which induced similarly strong adenosine responses in the mPFC, exhibited significant antidepressant effects at 5 mg kg^{-1}, whereas 3′-Cl-ketamine, which produced negligible adenosine responses, did not lead to improvements in depressive phenotypes at 10 mg kg^{-1} (Fig. 4h). These findings confirm that adenosine dynamics serve as a predictive biomarker for identifying ketamine-derived compounds with antidepressant efficacy.

We also used hyperlocomotion to evaluate the dissociative side effects of DCK. At a dose of 2 mg kg^{-1}, which effectively alleviated depressive-like behaviours, DCK induced only mild locomotor effects, which was in contrast to the significant hyperlocomotion observed with 10 mg kg^{-1} ketamine (Extended Data Fig. 8c,d). Higher doses of DCK caused more conspicuous motor activity, but the ability to achieve antidepressant effects at lower doses with minimal side effects underscores its favourable therapeutic window.

To determine whether NMDAR antagonism is the primary driver of adenosine release, we systematically compared the in vivo adenosine-releasing capacity of ketamine and six derivatives with their respective NMDAR inhibitory potencies (IC_{50}) and pharmacokinetics in the brain (Extended Data Fig. 9a–h). Our findings revealed a dissociation between these two properties. Notably, after integrating ex vivo potency with in vivo pharmacokinetics to estimate the effective NMDAR target engagement for each compound, we did not find a correlation between the degree of NMDAR blockade and the amplitude of the adenosine surge (Extended Data Fig. 9i). This was exemplified by compounds such as 3′-Cl-ketamine, which blocked NMDARs but did not trigger adenosine release, and 3C-DCK, which produced a much stronger release despite having comparable NMDAR affinity (Extended Data Fig. 9a,d,f). This dissociation between NMDAR antagonism and adenosine release, combined with our evidence that ketamine directly modulates mitochondrial metabolism (Extended Data Fig. 7), suggests that a non-NMDAR mechanism mediates the adenosine surge.

Adenosine mediates ECT and aIH action

Although ketamine represents a pharmacological intervention for rapid antidepressant effects, ECT offers a non-pharmacological approach with similarly rapid efficacy[3,41]. ECT induces epileptic and convulsive behaviours, characterized by neuronal hyperactivity, often linked to extracellular adenosine release as a protective mechanism against overexcitation. However, real-time adenosine dynamics during ECT remain unexplored. We monitored extracellular adenosine in the mPFC of anaesthetized mice undergoing ECT-induced seizures. ECT induced an increase in extracellular adenosine levels in the mPFC, comparable in magnitude to those produced with a 10 mg kg^{-1} intraperitoneal injection of ketamine, but with a faster onset and decay (Fig. 5a,b). An ECT regimen significantly alleviated depressive-like behaviours in mice subjected to CRS, as assessed by FSTs and SPTs, effects that were abolished in *Adora1*$^{-/-}$ and *Adora2a*$^{-/-}$ mice (Fig. 5c–e). These results highlight the essential role of adenosine signalling in ECT.

The connection between adenosine signalling and the antidepressant effects of ketamine and ECT points to the potential of non-pharmacological strategies such as aIH, which has demonstrated neuroprotective and anxiolytic benefits in both preclinical and clinical settings[42,43]. To replicate the adenosine surges observed with ketamine and ECT, we developed a controlled aIH protocol consisting of five 5-min exposures to 9% hypoxia, interspersed with 5-min normoxic intervals (21% O_2), administered once daily for three consecutive days. Fibre photometry revealed that aIH generated a rapid and significant increase in extracellular adenosine levels in the mPFC (Extended Data Fig. 10a,b). Behavioural assays demonstrated that this 3-day aIH regimen alleviated depression-like behaviours in mice subjected to CRS. These mice exhibited reduced immobility in FSTs and increased sucrose preference in SPTs, effects that were not seen in mice in which A_1 or A_{2A} receptors were genetically disrupted (Extended Data Fig. 10c–e). Notably, aIH treatment did not impair motor function or exercise capacity, which provides support for the safety of this strategy (Extended Data Fig. 10f). These findings indicate that aIH is a promising non-pharmacological therapy for depression, leveraging adenosine signalling to deliver rapid antidepressant effects with minimal side effects.

Discussion

Our study establishes adenosine signalling as a convergent mechanism for rapid-acting antidepressants that meets three key criteria: elevation in mood-regulatory circuits by ketamine and ECT; the necessity of A_1 and A_{2A} receptor activity for efficacy; and direct translatability to therapeutic design. Real-time monitoring revealed that these interventions induced adenosine surges in the brain (Figs. 1 and 5). Notably, this pathway is not merely correlational; receptor blockade abolished antidepressant effects, whereas receptor activation led to comparable responses (Figs. 2 and 5). Capitalizing on this mechanism, we engineered adenosine-enhancing ketamine derivatives that retained efficacy while attenuating psychotomimetic side effects (Fig. 4). We also demonstrated that aIH—a noninvasive strategy[42]—recapitulates antidepressant actions through adenosine signalling (Extended Data Fig. 10). This unified adenosine-centric framework positions adenosine signalling as a tractable target for mechanism-driven antidepressant development.

Ketamine, ECT and aIH produce their antidepressant effects through adenosine signalling, which selectively engages high-affinity, nanomolar-range A_1 and A_{2A} receptors over the low-affinity, micromolar-range A_{2B} and A_3 subtypes[24,28,29]. Optical recordings using the $GRAB_{ado1.0}$ sensor (EC_{50} of around 60 nM) revealed that the adenosine signals induced by ketamine and ECT were less than half the amplitude of those induced by transient hypoxia, which suggests that the unsaturated sensor responses correspond to local adenosine concentrations in the range of 100 nM. This level is sufficient to engage A_1 and A_{2A} receptors but remains substantially below the activation threshold for A_{2B} and A_3 receptors[24,28,29]. The causal necessity of this pathway was demonstrated by our findings that genetic or pharmacological disruption of either A_1 or A_{2A} receptor signalling abolished their therapeutic efficacy (Figs. 2 and 5 and Extended Data Figs. 3 and 10). A_1 receptor activation, which was sufficient to produce sustained antidepressant-like effects on its own, is thought to suppress neuronal hyperactivity via G_i-coupled signalling[24,28,29]. In parallel, G_s-coupled A_{2A} signalling promotes synaptic plasticity, in part by upregulating BDNF[44,45]. This dual-receptor signalling may provide a complementary upstream mechanism for previously implicated pathways, linking the action of ketamine to both mTOR activation and the induction of HOMER1A[5,20].

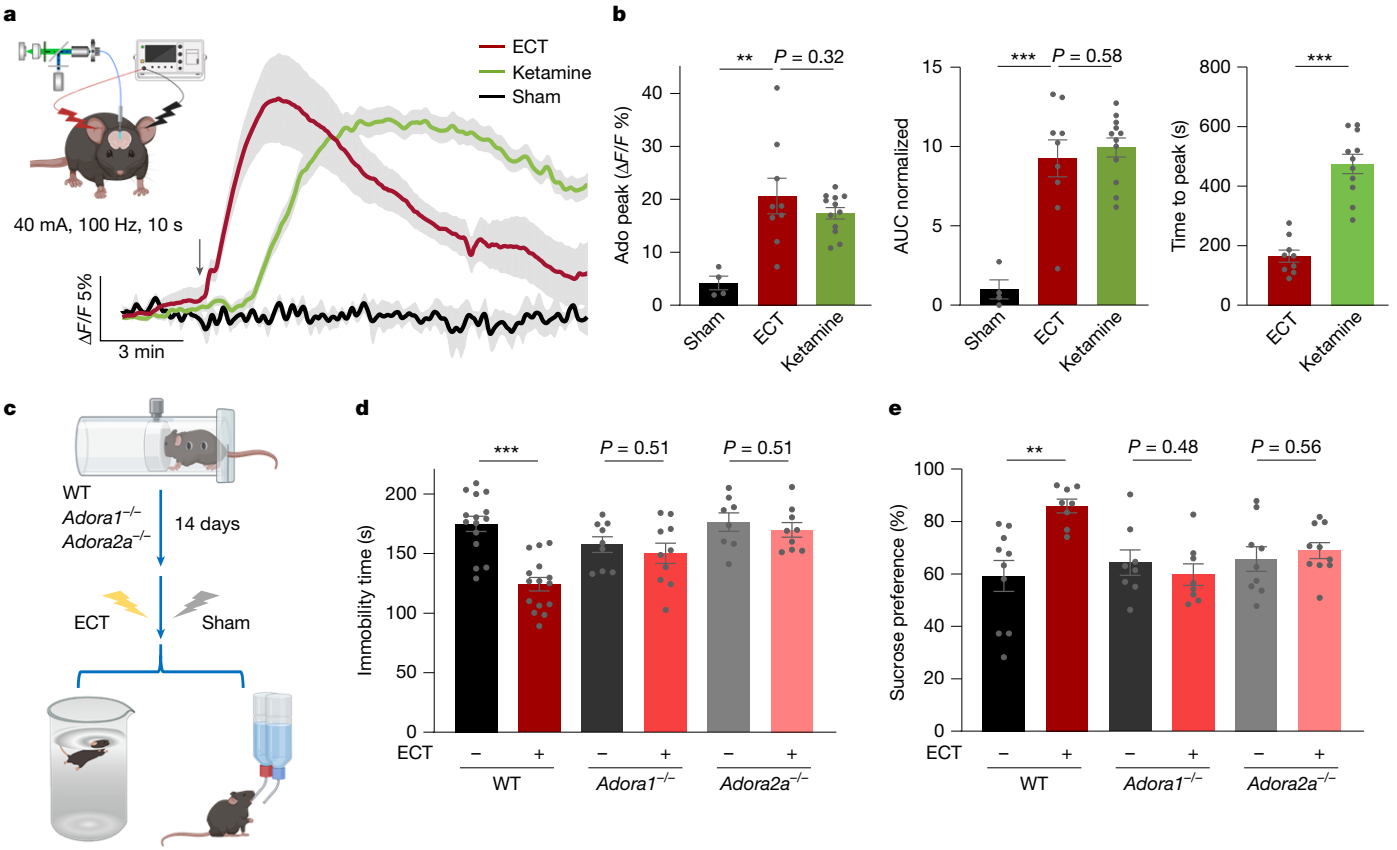

Fig. 5 | Adenosine signalling is essential for the antidepressant effects of ECT. a, Adenosine dynamics following ECT. Left, experimental setup for ECT in mice, showing ear-clamp electrodes for stimulation with concurrent $GRAB_{Ado1.0}$ monitoring. Right, extracellular adenosine time course in the mPFC after a single ECT cycle, ketamine injection (10 mg kg^{-1}, i.p. injection; replotted from Fig. 1e for comparison purpose) or sham ECT. Arrow indicates ECT or drug administration. **b**, Quantification of adenosine peak levels, AUC (normalized to sham ECT) and time to peak. **c**–**e**, Experimental paradigm for assessing ECT antidepressant efficacy (**c**), FST immobility time (**d**) and sucrose preference (**e**) of WT, *Adora1*$^{-/-}$ and *Adora2a*$^{-/-}$ mice subjected to CRS. Data are the mean ± s.e.m. (shading in **a**; error bars in **b**, **d** and **e**). Statistics: two-tailed unpaired *t*-tests (**b**,**d**,**e**). $^{**}P < 0.01$, $^{***}P < 0.001$. See Supplementary Table 1 for detailed statistics. The schematics in **a** and **c** were created using BioRender (https://www.biorender.com).

Our model also helps to reconcile the seemingly paradoxical role of the A_{2A} receptor, the chronic activity of which in the hippocampus and lateral septum is often linked to pro-depressive states[19,25]. Our findings indicate that the chronic, pathophysiological function of the A_{2A} receptor differs from its acute, instrumental role as a necessary component of the specific signalling cascade initiated by ketamine and ECT. Furthermore, this adenosine pathway is engaged by ketamine but not its metabolites (Extended Data Fig. 2), pointing towards a distinct, adenosine-independent mechanism for the potential effects of the latter. Thus, although the baseline activity of A_1 and A_{2A} receptors is context-dependent, their acute, coordinated activation is essential to initiate and sustain the neuroplastic changes that underlie recovery.

Circuit-level analyses identified the mPFC as the critical hub for these effects. Ketamine induced adenosine release selectively in the mPFC and hippocampus, but not the NAc (Fig. 1a,b and Extended Data Fig. 1c). Notably, adenosine signalling in the mPFC was both necessary and sufficient for antidepressant efficacy (Fig. 2f–i and Extended Data Fig. 5). Local adenosine infusion or optogenetic astrocyte activation in this region alleviated depression-like behaviours through CD73-dependent ATP-to-adenosine conversion, whereas mPFC-specific knockout of A_1 or A_{2A} receptors abolished the effects of ketamine. Although many studies suggest that the hippocampus contributes to the antidepressant action of ketamine[4,10,14,46,47], local adenosine signalling in the dorsal subregion was insufficient to drive this effect on its own (Extended Data Fig. 5f–j). This may reflect the known functional heterogeneity along the dorsoventral axis of the hippocampus, a complexity that warrants further investigation. Nevertheless, our findings establish the mPFC as a pivotal hub for this adenosine-mediated antidepressant efficacy.

Our findings further reveal that ketamine triggers this cascade by acting as a metabolic neuromodulator. Rather than causing neurotoxic ATP release from stressed cells, ketamine decreases the intracellular ATP/ADP ratio and directly attenuates mitochondrial TCA cycle activity (Fig. 3 and Extended Data Figs. 6 and 7). Owing to the large concentration gradient between millimolar intracellular ATP and nanomolar adenosine[23,36,37], a controlled brake on cellular metabolism can be amplified into potent adenosine signals. This mechanism informed our phenotypic drug discovery strategy, in which we engineered derivatives with enhanced adenosine release, greater efficacy and reduced side effects (Fig. 4). The clear dissociation between adenosine release and NMDAR inhibition provides an actionable blueprint for decoupling therapeutic benefits from psychomimetic actions, as demonstrated by the separation of antidepressant effects from hyperlocomotion (Extended Data Figs. 3b,c and 9).

The discovery that aIH also mediates its antidepressant effects through adenosine signalling (Extended Data Fig. 10) provides a promising non-pharmacological avenue. Unlike ECT, which induces seizures and carries risks of cognitive impairment[3,15], or repetitive transcranial magnetic stimulation, which has limited efficacy in treatment-resistant cases[48,49], aIH is a noninvasive strategy with an established safety profile in humans[42]. Its ability to elevate brain adenosine presents an opportunity to repurpose this protocol for treatment-resistant depression.

In summary, adenosine signalling emerges as a conserved mediator of rapid antidepressant efficacy across pharmacological, electrical

and physiological interventions. Our findings highlight key clinical considerations, such as the potential for dietary caffeine to interfere with these treatments[49,50], and provide a unified framework to accelerate the development of safer, mechanism-targeted antidepressants with broad clinical applicability.

Online content

Any methods, additional references, Nature Portfolio reporting summaries, source data, extended data, supplementary information, acknowledgements, peer review information; details of author contributions and competing interests; and statements of data and code availability are available at https://doi.org/10.1038/s41586-025-09755-9.

1. Berman, R. M. et al. Antidepressant effects of ketamine in depressed patients. *Biol. Psychiatry* **47**, 351–354 (2000).
2. Zarate, C. A. Jr et al. A randomized trial of an *N*-methyl-D-aspartate antagonist in treatment-resistant major depression. *Arch. Gen. Psychiatry* **63**, 856–864 (2006).
3. Lisanby, S. H. Electroconvulsive therapy for depression. *N. Engl. J. Med.* **357**, 1939–1945 (2007).
4. Autry, A. E. et al. NMDA receptor blockade at rest triggers rapid behavioural antidepressant responses. *Nature* **475**, 91–95 (2011).
5. Li, N. et al. mTOR-dependent synapse formation underlies the rapid antidepressant effects of NMDA antagonists. *Science* **329**, 959–964 (2010).
6. Aguilar-Valles, A. et al. Antidepressant actions of ketamine engage cell-specific translation via eIF4E. *Nature* **590**, 315–319 (2021).
7. Casarotto, P. C. et al. Antidepressant drugs act by directly binding to TRKB neurotrophin receptors. *Cell* **184**, 1299–1313 (2021).
8. Moda-Sava, R. N. et al. Sustained rescue of prefrontal circuit dysfunction by antidepressant-induced spine formation. *Science* **364**, eaat8078 (2019).
9. Kim, J. W., Suzuki, K., Kavalali, E. T. & Monteggia, L. M. Ketamine: mechanisms and relevance to treatment of depression. *Annu. Rev. Med.* **75**, 129–143 (2024).
10. Zanos, P. et al. NMDAR inhibition-independent antidepressant actions of ketamine metabolites. *Nature* **533**, 481–486 (2016).
11. Yang, Y. et al. Ketamine blocks bursting in the lateral habenula to rapidly relieve depression. *Nature* **554**, 317–322 (2018).
12. Anis, N. A., Berry, S. C., Burton, N. R. & Lodge, D. The dissociative anaesthetics, ketamine and phencyclidine, selectively reduce excitation of central mammalian neurones by *N*-methyl-aspartate. *Br. J. Pharmacol.* **79**, 565–575 (1983).
13. Zanos, P. & Gould, T. D. Mechanisms of ketamine action as an antidepressant. *Mol. Psychiatry* **23**, 801–811 (2018).
14. Krystal, J. H., Abdallah, C. G., Sanacora, G., Charney, D. S. & Duman, R. S. Ketamine: a paradigm shift for depression research and treatment. *Neuron* **101**, 774–778 (2019).
15. Leaver, A. M., Espinoza, R., Wade, B. & Narr, K. L. Parsing the network mechanisms of electroconvulsive therapy. *Biol. Psychiatry* **92**, 193–203 (2022).
16. Dunwiddie, T. V. & Masino, S. A. The role and regulation of adenosine in the central nervous system. *Annu. Rev. Neurosci.* **24**, 31–55 (2001).
17. Chen, J. F., Lee, C. F. & Chern, Y. Adenosine receptor neurobiology: overview. *Int. Rev. Neurobiol.* **119**, 1–49 (2014).
18. Fries, G. R., Saldana, V. A., Finnstein, J. & Rein, T. Molecular pathways of major depressive disorder converge on the synapse. *Mol. Psychiatry* **28**, 284–297 (2023).
19. van Calker, D., Biber, K., Domschke, K. & Serchov, T. The role of adenosine receptors in mood and anxiety disorders. *J. Neurochem.* **151**, 11–27 (2019).
20. serchov, t. et al. Increased signaling via adenosine A_1 receptors, sleep deprivation, imipramine, and ketamine inhibit depressive-like behavior via induction of Homer1a. *Neuron* **87**, 549–562 (2015).
21. Hines, D. J., Schmitt, L. I., Hines, R. M., Moss, S. J. & Haydon, P. G. Antidepressant effects of sleep deprivation require astrocyte-dependent adenosine mediated signaling. *Transl. Psychiatry* **3**, e212 (2013).
22. Masino, S. A., Kawamura, M., Wasser, C. D., Pomeroy, L. T. & Ruskin, D. N. Adenosine, ketogenic diet and epilepsy: the emerging therapeutic relationship between metabolism and brain activity. *Curr. Neuropharmacol.* **7**, 257–268 (2009).
23. Latini, S. & Pedata, F. Adenosine in the central nervous system: release mechanisms and extracellular concentrations. *J. Neurochem.* **79**, 463–484 (2001).
24. Borea, P. A., Gessi, S., Merighi, S., Vincenzi, F. & Varani, K. Pharmacology of adenosine receptors: the state of the art. *Physiol. Rev.* **98**, 1591–1625 (2018).
25. Wang, M. et al. Lateral septum adenosine A_{2A} receptors control stress-induced depressive-like behaviors via signaling to the hypothalamus and habenula. *Nat. Commun.* **14**, 1880 (2023).
26. Winn, H. R., Rubio, R. & Berne, R. M. Brain adenosine concentration during hypoxia in rats. *Am. J. Physiol.* **241**, H235–H242 (1981).
27. Dinis-Oliveira, R. J. Metabolism and metabolomics of ketamine: a toxicological approach. *Forensic Sci. Res.* **2**, 2–10 (2017).
28. Jacobson, K. A. & Gao, Z. G. Adenosine receptors as therapeutic targets. *Nat. Rev. Drug Discov.* **5**, 247–264 (2006).
29. Chen, J. F., Eltzschig, H. K. & Fredholm, B. B. Adenosine receptors as drug targets—what are the challenges? *Nat. Rev. Drug Discov.* **12**, 265–286 (2013).
30. Lazarevic, V., Yang, Y., Flais, I. & Svenningsson, P. Ketamine decreases neuronally released glutamate via retrograde stimulation of presynaptic adenosine A_1 receptors. *Mol. Psychiatry* **26**, 7425–7435 (2021).
31. Cunha, M. P. et al. Creatine, similarly to ketamine, affords antidepressant-like effects in the tail suspension test via adenosine A_1 and A_{2A} receptor activation. *Purinergic Signal.* **11**, 215–227 (2015).
32. Walker, A. K. et al. NMDA receptor blockade by ketamine abrogates lipopolysaccharide-induced depressive-like behavior in C57BL/6J mice. *Neuropsychopharmacology* **38**, 1609–1616 (2013).
33. Li, H. et al. Astrocytes release ATP/ADP and glutamate in flashes via vesicular exocytosis. *Mol. Psychiatry* **30**, 2475–2489 (2025).
34. Bjorkholm, C. & Monteggia, L. M. BDNF—a key transducer of antidepressant effects. *Neuropharmacology* **102**, 72–79 (2016).
35. Kim, J. W. et al. Sustained effects of rapidly acting antidepressants require BDNF-dependent MeCP2 phosphorylation. *Nat. Neurosci.* **24**, 1100–1109 (2021).
36. Yegutkin, G. G. Nucleotide- and nucleoside-converting ectoenzymes: important modulators of purinergic signalling cascade. *Biochim. Biophys. Acta* **1783**, 673–694 (2008).
37. Berg, J., Hung, Y. P. & Yellen, G. A genetically encoded fluorescent reporter of ATP:ADP ratio. *Nat. Methods* **6**, 161–166 (2009).
38. Garcia-Gil, M., Camici, M., Allegrini, S., Pesi, R. & Tozzi, M. G. Metabolic aspects of adenosine functions in the brain. *Front. Pharmacol.* **12**, 672182 (2021).
39. Zanos, P. et al. Ketamine and ketamine metabolite pharmacology: insights into therapeutic mechanisms. *Pharmacol. Rev.* **70**, 621–660 (2018).
40. Fond, G. et al. Ketamine administration in depressive disorders: a systematic review and meta-analysis. *Psychopharmacology* **231**, 3663–3676 (2014).
41. Kellner, C. H. et al. ECT in treatment-resistant depression. *Am. J. Psychiatry* **169**, 1238–1244 (2012).
42. Navarrete-Opazo, A. & Mitchell, G. S. Therapeutic potential of intermittent hypoxia: a matter of dose. *Am. J. Physiol. Regul. Integr. Comp. Physiol.* **307**, R1181–R1197 (2014).
43. Duszczyk, M. et al. Antidepressant-like and anxiolytic-like effects of mild hypobaric hypoxia in mice: possible involvement of neuropeptide Y. *Acta Neurobiol. Exp.* **75**, 364–371 (2015).
44. Tebano, M. T. et al. Adenosine A_{2A} receptors are required for normal BDNF levels and BDNF-induced potentiation of synaptic transmission in the mouse hippocampus. *J. Neurochem.* **104**, 279–286 (2008).
45. Fontinha, B. M., Diogenes, M. J., Ribeiro, J. A. & Sebastiao, A. M. Enhancement of long-term potentiation by brain-derived neurotrophic factor requires adenosine A_{2A} receptor activation by endogenous adenosine. *Neuropharmacology* **54**, 924–933 (2008).
46. Su, T., Lu, Y., Fu, C., Geng, Y. & Chen, Y. GluN2A mediates ketamine-induced rapid antidepressant-like responses. *Nat. Neurosci.* **26**, 1751–1761 (2023).
47. Duman, R. S., Aghajanian, G. K., Sanacora, G. & Krystal, J. H. Synaptic plasticity and depression: new insights from stress and rapid-acting antidepressants. *Nat. Med.* **22**, 238–249 (2016).
48. Somani, A. & Kar, S. K. Efficacy of repetitive transcranial magnetic stimulation in treatment-resistant depression: the evidence thus far. *Gen. Psychiatr.* **32**, e100074 (2019).
49. Lopes, J. P., Pliassova, A. & Cunha, R. A. The physiological effects of caffeine on synaptic transmission and plasticity in the mouse hippocampus selectively depend on adenosine A_1 and A_{2A} receptors. *Biochem. Pharmacol.* **166**, 313–321 (2019).
50. Fredholm, B. B., Battig, K., Holmen, J., Nehlig, A. & Zvartau, E. E. Actions of caffeine in the brain with special reference to factors that contribute to its widespread use. *Pharmacol. Rev.* **51**, 83–133 (1999).

Methods

Mice

All animal procedures were performed in accordance with protocols approved by the Institutional Animal Care and Use Committee of the Chinese Institute for Brain Research, Beijing (CIBR), and complied with the national guidelines for the housing and care of laboratory animals set by the Ministry of Health, China. Mice were housed in a specific pathogen-free facility on a 12-h light–dark cycle with ad libitum access to food and water. All experiments were conducted on male and female mice aged 8–16 weeks.

The study used WT C57BL/6J mice, *Adora1*$^{-/-}$ mice (NM-KO-225140, Shanghai Model Organisms Center), *Adora2a*$^{-/-}$ mice (NM-KO-200018, Shanghai Model Organisms Center), *Nt5e*$^{-/-}$ mice (provided by J. Chen, Wenzhou Medical University) and Rosa26-Cas9-GFP mice (*Gt(ROSA)26Sor*$^{tm1.1(CAG-cas9*,-EGFP)Fezh}$/J; The Jackson Laboratory, 024858). All mouse strains were subjected to CRS to induce depression, and WT, *Nt5e*$^{-/-}$, *Adora1*$^{-/-}$ and *Adora2a*$^{-/-}$ mice were used for fibre photometry experiments.

Chemical reagents

Ketamine analogues were synthesized and provided by the Changchun Institute of Applied Chemistry, CAS, China (see below). Additional key chemicals were purchased from commercial sources, including norketamine hydrochloride (Tocris, 1970), (2*R*,6*R*)-HNK (Tocris, 6094), ticlopidine (Selleck, S0721), ketoconazole (Selleck, S1353), ritonavir (Selleck, S1185), dipyridamole (Selleck, S1895), LPS from *Escherichia coli* O127:B8 (LPS; Sigma, L3129), PSB36 (MCE, HY-103175), ZM241385 (Selleck, S8105), CHA (MCE, HY-18939), CGS21680 hydrochloride (MCE, HY-13201A), adenosine (MCE, HY-B0228), sodium [$^{13}C_3$]pyruvate (MCE, HY-W015913S), ADP (MCE, HY-W010918) and wheat germ agglutinin (Alexa Fluor 555; Thermo Scientific, W32464).

Compound synthesis and characterization

Full experimental procedures, compound characterization data (^{1}H NMR and ^{13}C NMR) and analytical spectra are provided in the Supplementary Information. A summary of the synthesis for the two key compounds (DCK and 2C-DCK) is presented below.

For the general procedure for the synthesis of 2-aryl-2-bromo-cycloketones, *N*-bromosuccinimide (1.5 equiv.) and dimethyl sulfoxide (2.0 equiv.) were added to a solution of 2-arylcyclohexan-1-one (1.0 equiv.) in $CHCl_3$. The reaction mixture was stirred at room temperature and monitored by thin-layer chromatography. After completion, the reaction was quenched with saturated aqueous $Na_2S_2O_3$ and water. The aqueous phase was extracted with CH_2Cl_2 (3 times). The combined organic layers were dried over anhydrous Na_2SO_4, filtered and concentrated under reduced pressure. The crude product was purified by flash column chromatography (petroleum ether/ethyl acetate) to afford the desired 2-aryl-2-bromo-cycloketone.

For the general procedure for the synthesis of ketamine derivatives (DCK and 2C-DCK), a solution of the appropriate 2-aryl-2-bromo-cycloketone (1.0 mmol) in anhydrous THF was cooled to the specified temperature (−25 °C) under a nitrogen atmosphere. The corresponding amine (methylamine for DCK; ethylamine for 2C-DCK; 4.0 equiv.) was added, and the reaction was stirred until thin-layer chromatography indicated complete consumption of the starting material. The reaction was quenched by the addition of saturated aqueous Na_2CO_3 and water. The mixture was extracted with CH_2Cl_2 (3 times), and the combined organic layers were dried over anhydrous Na_2SO_4. The solvent was removed in vacuo, and the residue was treated with diethyl ether and aqueous HCl. The aqueous layer was washed with diethyl ether, neutralized with saturated aqueous Na_2CO_3 and extracted with CH_2Cl_2 (3 times). The final organic layers were combined, dried over anhydrous Na_2SO_4 and concentrated to dryness under vacuum to produce the final product.

Below are the characterizations of DCK and 2C-DCK using NMR spectroscopy.

Compound 2 (DCK): 2-(Methylamino)–2-phenylcyclohexan-1-one. ^{1}H NMR (300 MHz, $CDCl_3$): δ 7.45–7.34 (m, 2H), 7.33–7.19 (m, 3H), 3.01–2.79 (m, 1H), 2.48–2.19 (m, 3H), 2.03 (s, 3H), 2.01–1.91 (m, 1H), 1.90–1.61 (m, 4H). ^{13}C NMR (75 MHz, $CDCl_3$): δ 211.7, 138.9, 128.9, 127.6, 127.2, 70.0, 39.9, 35.5, 29.0, 27.9, 22.4.

Compound 3 (2C-DCK): 2-(ethylamino)–2-phenylcyclohexan-1-one. ^{1}H NMR (300 MHz, $CDCl_3$) δ 7.42–7.33 (m, 2H), 7.31–7.20 (m, 3H), 2.90 (d, *J* = 11.0 Hz, 1H), 2.50–2.22 (m, 3H), 2.16 (s, 1H), 2.11–2.01 (m, 1H), 2.01–1.60 (m, 5H), 0.99 (t, *J* = 7.1 Hz, 3H). ^{13}C NMR (75 MHz, $CDCl_3$): δ 211.5, 139.5, 128.9, 127.5, 127.1, 69.9, 39.8, 36.6, 36.1, 27.8, 22.4, 15.7.z.

AAV vectors

The following AAV vectors were produced in-house (M.L's laboratory) by co-transfecting HEK293T cells with the following respective AAV plasmid and helper plasmids: AAV2/9-hSyn-GRAB$_{Ado1.0}$, AAV2/9-EF1a-DIO-GCaMP8s, AAV2/8-GfaABC1D-GRAB$_{ATP1.0}$ and AAV2/8-GfaABC1D-cOpsin5-T2A-mCherry. Viral particles were purified by cesium chloride density gradient ultracentrifugation, dialysed into PBS and titred by quantitative PCR (qPCR) to 5–15 × 10^{12} viral genomes per ml[51].

The following additional vectors were obtained: AAV-hSyn-GRAB$_{Ado1.0\text{-}mut}$ was generated in Y.L's Laboratory; AAV-EF1α-DIO-PercevalHR and AAV2/5-GfaABC1D-PercevalHR were produced in Z.W's laboratory; and AAV2/8-GfaABC1D-mCherry was purchased from Taitool Bioscience.

For conditional knockout in the mPFC, sgRNAs targeting *Adora1* (5′-GTGTAGCGGTAGCCAGCTGA-3′, 5′-CCGGAACTTGTGGATTCGGA-3′ and 5′-GATCAAGTGTGAGTTCGAGA-3′) and *Adora2a* (5′-TCGCC ATCCGAATTCCACTC-3′, 5′-TCTGGCGGCGGCTGACATCG-3′ and 5′-AGCACACAAGCACGTTACCC-3′) were designed. Non-targeting control sgRNAs (5′-GCGAGGTATTCGGCTCCGCG-3′, 5′-GCTTTCACGG AGGTTCGACG-3′ and 5′-ATGTTGCAGTTCGGCTCGAT-3′) were also used. Each sgRNA, driven by a U6 promoter, was co-packaged with a CMV-driven saCas9-3×HA into either AAV2/9 (for neuronal targeting) or AAV2/8 (for astrocytic targeting) vectors.

Validation of global *Adora1* and *Adora2a* knockout and mPFC-specific knockdown was performed using qPCR on cDNA from brain tissues with the following primer pairs: *Adora1* knockout (F: 5′-TGTGCC CGGAAATGTACTGG-3′, R: 5′-TCTGTGGCCCAAATGTTGATAAG-3′); *Adora2a* knockout (F: 5′-GTGCTGTCATTCGCCATCGG-3′, R: 5′-GGGAGC AACACAAAAGCGAAG-3′); *Adora1* sgRNA for conditional knockdown (F: 5′-GCCAGAAACCCAGCATCCTC-3′, R: 5′-CAGAAAGGTGACCCGG AACT-3′); and *Adora2a* sgRNA (F: 5′-GCCATCCCATTCGCCATCA-3′, R: 5′-GCAATAGCCAAGAGGCTGAAGA-3′). All primers were designed to span critical exon junctions or CRISPR–Cas9-targeted regions, with reaction specificity confirmed by melt curve analysis and agarose gel electrophoresis. qPCR was carried out in triplicate using SYBR Green chemistry under standard cycling conditions.

Surgical procedures

Mice were anaesthetized with avertin (250 mg kg^{-1}, i.p. injection) and secured in a stereotaxic apparatus (RWD). Following skull exposure, a small craniotomy was made above the target region. AAV injections were performed using a microsyringe pump (Nanoliter 2010 Injector, WPI) at a rate of 46 nl min^{-1} via a glass pipette. Injection coordinates (anterior–posterior (AP), medial–lateral (ML), dorsal–ventral (DV) in mm from bregma) were as follows: PrL and IL in the mPFC (+1.78, ±0.88, −2.15, respectively) with a 15° lateral-to-medial angle; ACC (+1.15, ±0.70, −1.47, respectively) with a 15° lateral-to-medial angle; HPC (−2.54, ±2.00, −1.60, respectively) and NAc (+1.20, ±1.20, −4.65, respectively).

For fibre photometry and optogenetic stimulation experiments[52,53], optical fibre implantation was performed after viral injection. Optical

fibres (FT200UMT, Thorlabs) mounted in ceramic ferrules were positioned above the mPFC, ACC, HPC or NAc, with the tip located 0.1 mm above the injection site. For intracranial adenosine injection, a cannula (62004, RWD) was implanted into the lateral ventricle (AP: −0.45, ML: −1.84, DV: −2.45 DV) at a 15° lateral-to-medial angle.

For in vivo two-photon imaging, mice were imaged 14 days after viral injection to allow time for virus expression. Subsequently, under anaesthesia, a 3-mm diameter skull aperture was drilled at the injection site and covered with a glass window. A stainless-steel head-restraining bar integrated with an imaging chamber was affixed with dental cement. Mice recovered for 1 week before imaging, which was conducted in the awake state.

Fibre photometry

In vivo fluorescence signals from $GRAB_{Ado1.0}$, $GRAB_{Ado1.0\text{-}mut}$, $GRAB_{ATP1.0}$ and GCamp8s signals were recorded using a multichannel fibre photometry system[54,55] (ThinkerTech). A 470-nm blue LED provided sensor excitation, with the intensity adjusted to minimize photobleaching. The resulting emission was passed through a dichroic mirror (MD498, Thorlabs) and a bandpass filter (525 ± 19.5 nm; MF525−39, Thorlabs) before detection.

Fibre photometry of PercevalHR signals was conducted on a separate two-colour multichannel optical fibre photometry system (Optical Imaging Facility, CIBR). To measure the intracellular ATP/ADP ratio, the PercevalHR sensor was alternately excited at 405 nm and 470 nm, with emission collected at 525 nm, as previously described[37,56]. The ratio of fluorescence intensity from 470 nm excitation to that from 405 nm excitation (F_{470}/F_{405}) was calculated to represent changes in the ATP/ADP ratio.

For pharmacological studies, mice implanted with an optical fibre were habituated for 15–20 min in a behaviour chamber (20 × 20 × 35 cm) to establish a baseline signal. Following habituation, the mice given an i.p. injection of the drug of interest, and fluorescence signals were continuously recorded. Animal behaviour was monitored using a top-mounted camera.

For acute hypoxia experiments, mice were placed in a cylindrical chamber with ports for the optical fibre, gas flow and an oxygen sensor (ST8100A, Smart Sensor). After a 20-min acclimation period with a continuous flow of air (21% O_2), hypoxia was induced by mixing the room air with 100% N_2 via a three-way valve. $GRAB_{Ado1.0}$ and $GRAB_{Ado1.0\text{-}mut}$ signals were continuously recorded during acclimation, hypoxia and subsequent reoxygenation with air. After the trial, the chamber was cleaned with 70% ethanol and dried.

Fibre photometry data were analysed using custom Matlab scripts. Fluorescence changes were calculated as $\Delta F/F = (F - F_0)/F_0$, where F_0 represents the mean fluorescence during a baseline period before drug administration. For recordings longer than 30 min, photobleaching was corrected by subtracting a 'blank' signal, which was recorded from the same animals on a separate day without any drug or saline administration. From the resulting $\Delta F/F$ traces, the following parameters were quantified: peak amplitude, the maximum signal intensity reached after stimulation or drug administration; time to peak, the latency from administration to the peak amplitude; onset time, the time for the signal to reach 20% of the peak amplitude; rise time, the interval during which the signal increased from 20% to 90% of its peak; and decay time, the time taken for the signal to decrease to 50% of its peak amplitude.

In vivo two-photon imaging

During imaging sessions, mice remained awake and were gently restrained using a custom-built head-fixation device. Images were acquired 100–150 μm below the dura mater using a Stellaris 8 Dive multiphoton microscope (Leica, ×25 water-immersion lens with NA 1.05). The microscope was calibrated for consistent illumination and exposure settings across all imaging sessions. A 20-min baseline was recorded before ketamine (10 mg kg^{-1}, i.p. injection) or an equivalent volume of saline as a control was given. Following the injection, imaging continued for an additional 20 min to capture changes in neural activity.

To correct for lateral shifts in two-photon images, we used the Image Stabilizer plugin in ImageJ (Fiji, v.2.14.0). For time trace analyses of fluorescence signals based on the region of interest, the Time Series Analyzer V3 plugin in ImageJ was used. $\Delta F/F$ values were calculated using customized Matlab scripts (MathWorks), and heatmaps or time traces were generated accordingly. Statistical significance was assessed using Prism 9 (GraphPad Software). All data are reported as the mean ± s.e.m. in the figures.

Confocal imaging of $GRAB_{Ado1.0}$ in cultured cells

HEK293T cells were cultured on 35-mm poly-D-lysine-coated glass-bottom dishes (NEST, 801002). At 60–70% confluency, cells were transfected with the $GRAB_{Ado1.0}$ plasmid using Neofect DNA transfection reagent (Neofect Biotech). Imaging was performed 48 h after transfection on a Zeiss LSM 880 inverted confocal microscope (Carl Zeiss) using a ×20/0.8 NA Plan-Apochromat objective. The $GRAB_{Ado1.0}$ sensor was excited with a 488-nm argon laser.

Behavioural assays

All behavioural assays were performed on animals 12–16 weeks old. Most behavioural assays were performed during the light phase, except for the SPT, which was performed during the dark phase to maximize the consumption of solution. Behavioural analyses were performed blinded to experimental conditions.

CRS assay. Mice were subjected to an environmental acclimation period of 3 days preceding initiation of the experiment. Subsequently, the mice were immobilized utilizing custom-fabricated restraining tubes (50 ml centrifuge tubes) with ventilation apertures to ensure the maintenance of normal respiration. The restraint protocol was implemented for a duration ranging from 4 to 6 h per day over a consecutive 14-day period[57]. After completion of the modelling phase, a behavioural experiment was conducted for the purpose of assessment.

LPS-induced inflammatory depression model. The LPS-induced depression model is a well-established paradigm for rapidly inducing depressive-like behaviours in mice[32]. In brief, i.p. administration of a low dose of LPS (0.83 mg kg^{-1}, *E. coli* O127:B8, Sigma-Aldrich) induces a mild inflammatory response and triggers transient sickness behaviour within 24 h. Subsequently, between 24 and 72 h after injection, mice develop persistent depression-like phenotypes, including anhedonia, behavioural despair and anxiety-like responses.

FST assay. Mice were individually placed into Plexiglass cylinders (26.5 cm high × 18 cm in diameter) containing 14 cm of water maintained at 25 ± 1 °C. The test lasted for 6 min under standard illumination, with a digital video camera recording from the side. Immobility time during the final 4 min of the test, defined as the period during which mice floated passively with only minimal movements necessary to maintain balance, was scored by a trained observer blinded to the experimental treatments[58].

SPT assay. Mice were habituated to two bottles of drinking water in their home cages for 2 days, followed by exposure to two bottles containing 2% sucrose solution for an additional 2 days. After habituation, mice were deprived of water for 24 h and then presented with one bottle of 1% sucrose solution and one bottle of water for 2 h during the dark phase. The positions of the bottles were switched after 1 h to control for side preference. Sucrose preference was calculated as the percentage of sucrose intake relative to the total fluid intake (sucrose and water combined)[59].

Open-field test. Locomotor activity was assessed using an infrared open-field system (Med Associates; 50 × 50 × 30 cm). Baseline activity was measured in WT, *Adora1*$^{-/-}$ and *Adora2a*$^{-/-}$ mice during a 10-min session. Mice were placed at the centre of the arena, and total travel distance was recorded using an automated tracking system. To evaluate the effects of ketamine and DCK, mice were acclimated for 15 min in the arena, followed by drug administration. Locomotor activity was monitored for 75 min after treatment, with total travel distance recorded over the 90-min session. In a separate experiment, WT, *Adora1*$^{-/-}$ and *Adora2a*$^{-/-}$ mice underwent the same acclimation period (15 min) followed by ketamine and saline administration, with activity recorded for 30 min after treatment.

ECT in mice. Following CRS, mice were anaesthetized with avertin, and their ears were cleaned with 70% ethanol. ECT was delivered via ear-clip electrodes using a YC-3 Bipolar Programmable Stimulator, applying an electrical current of 40 mA (100 Hz, 10-s duration, 0.5-ms pulse width)[60]. This stimulation induced a tonic–clonic seizure lasting approximately 10 s. Sham-treated animals underwent identical handling, including electrode attachment, but no current was delivered.

aIH treatment. Mice subjected to CRS were exposed to aIH using an interval conditioning regimen[42]. The regimen comprised five cycles of a 5-min hypoxia period at 9% O_2, each followed by a 5-min normoxic interval (21% O_2), repeated daily for three consecutive days. The oxygen concentration was monitored in real time using an integrated sensor (ST8100A, Smart Sensor). The antidepressant effects of aIH were assessed using established models of depressive-like behaviour, including the FST and SPT. For fibre photometry recordings of adenosine dynamics, a 15-min baseline recording was performed before aIH exposure to monitor signal changes in response to the interval training protocol.

Local drug infusion

Bilateral 26-gauge guide cannulae (RWD Life Science) were stereotaxically implanted to target the mPFC (AP: +1.78 mm, ML: ±0.5 mm, DV: −2.05 mm from bregma) and the HPC (AP: −2.54 mm, ML: ±2.00 mm, DV: −1.60 mm). Following a 7-day postoperative recovery period, during which dummy cannulae maintained patency, mice were subjected to a 2-week CRS paradigm. For microinfusions, adenosine (0.1 μg μl^{-1}) were dissolved in sterile 0.9% saline. Solutions were delivered bilaterally (1 μl per side) at a rate of 0.2 μl min^{-1} via 33-gauge injectors connected to a microsyringe pump. The injectors remained in place for 7 min after infusion to allow for diffusion. Behavioural testing, using either the FST or SPT, was conducted 24 h after ketamine administration. At the conclusion of all experiments, cannula placement was histologically verified following the infusion of wheat germ agglutinin conjugated to Alexa Fluor 555 (WGA-555; 1 μl per side; Thermo Fisher Scientific).

Optogenetics

WT and *Nt5e*$^{-/-}$ mice previously subjected to CRS were used for optogenetic experiments. Animals were injected with AAVs expressing either AAV-GfaABC1D-cOpn5-T2A-mCherry (cOpn5 group) or AAV-GfaABC1D-mCherry (control group) in the target brain region. For stimulation, blue light (473 nm; MBL-III-473, Changchun New Industries Optoelectronics) was delivered through the implanted optical fibre at 20 Hz for 10 min (peak power at fibre tip: 0.75 mW)[61]. Stimulation timing was controlled by a Master-8 pulse generator (AMPI). FSTs and SPTs were performed 1 h after the cessation of stimulation to assess antidepressant-like effects.

LC–MS quantification of drug concentrations

WT mice were administered either adenosine receptor agonists or ketamine derivatives. At specified time points after injection (10 min for ketamine derivatives; 30 min or 24 h for agonists), mice were deeply anaesthetized with isoflurane. Whole blood was collected via retro-orbital bleeding, and mice were subsequently transcardially perfused with ice-cold PBS. Brain tissue was rapidly dissected, weighed and flash-frozen in liquid nitrogen. Blood samples were allowed to clot at room temperature and then centrifuged at 3,500*g* for 10 min at 4 °C to separate the serum. For analysis, serum proteins were precipitated by adding four volumes of acetonitrile to one volume of serum, followed by vortexing and centrifugation. Brain tissue was homogenized in 80% acetonitrile using a bead-based homogenizer, and the resulting lysate was clarified by centrifugation. Supernatants from both serum and brain preparations were diluted 100-fold with 80% acetonitrile. Drug concentrations were then quantified using a SCIEX 7500 triple quadrupole mass spectrometer.

Mitochondrial metabolic flux analysis

Mitochondrial isolation. Mitochondria were isolated from the prefrontal cortex of adult mice using a commercial kit (EpiZyme, PC205) with minor modifications. In brief, dissected tissue was homogenized, and crude mitochondria were pelleted by differential centrifugation. Highly purified mitochondria were then obtained by density gradient centrifugation according to the manufacturer's protocol, washed and resuspended for downstream assays.

Metabolic modulation and metabolite extraction. Purified mitochondria were incubated for 30 min at 37 °C in an intracellular buffer containing sodium [$^{13}C_3$]pyruvate and ADP, with or without ketamine at various concentrations. Following incubation, mitochondria were pelleted, and metabolites were extracted using cold (−40 °C) 50% aqueous methanol solution followed by phase separation with chloroform. The resulting aqueous phase, containing polar metabolites, was collected for analysis.

LC–MS-based metabolomics. Metabolite profiling was performed using hydrophilic interaction chromatography (HILIC) on an XBridge BEH Amide column (Waters) coupled to a Q Exactive Plus Orbitrap mass spectrometer (Thermo Fisher Scientific). Samples were separated using a gradient of aqueous ammonium acetate/hydroxide (pH 9.4) and acetonitrile. Mass spectrometry was operated in negative ion mode at a resolution of 140,000 (*m/z* 200), with an AGC target of 1×10^6 and a scan range of *m/z* 75–1,000. Metabolite identification, quantification and isotopic tracing were conducted using El-MAVEN software, with correction for natural isotope abundance. We performed PCA of the metabolomic data and defined ellipse 95% confidence intervals based on the multivariate *t*-distribution (Fig. 3h). The corresponding source data and analysis code are provided in the source files.

Ex vivo electrophysiology

Mice (C57BL/6J mice, 7–8 weeks old) were anaesthetized with an overdose of avertin and transcardially perfused with ice-cold, oxygenated choline-based slicing solution (in mM: 110 choline chloride, 2.5 KCl, 0.5 $CaCl_2$, 7 $MgCl_2$, 1.3 NaH_2PO_4, 25 $NaHCO_3$, 10 glucose, 1.3 sodium ascorbate and 0.6 sodium pyruvate). Coronal brain slices (200 μm) containing the mPFC were prepared using a vibratome (Leica VT1200). Slices were first recovered at 34 °C for 40 min in oxygenated artificial cerebrospinal fluid (ACSF; in mM: 125 NaCl, 2.5 KCl, 2 $CaCl_2$, 1.3 $MgCl_2$, 1.3 NaH_2PO_4, 1.3 sodium ascorbate, 0.6 sodium pyruvate, 10 glucose and 25 $NaHCO_3$) and then maintained at room temperature for at least 1 h before recording.

Whole-cell patch-clamp recordings were performed in Mg^{2+}-free ACSF to relieve the voltage-dependent block of NMDARs. Recording pipettes (4–6 MΩ) were filled with a caesium-based internal solution (in mM: 115 $CsMeSO_3$, 20 CsCl, 10 HEPES, 2.5 $MgCl_2$, 4 sodium ATP, 0.4 sodium GTP, 10 sodium phosphocreatine, 0.6 EGTA and 5 QX-314; pH 7.25–7.30). To isolate NMDAR-mediated excitatory postsynaptic currents (eEPSCs), recordings were performed in the presence of NBQX (10 μM, MCE) and picrotoxin (100 μM, Tocris). eEPSCs were evoked

by local stimulation (0.4-ms pulse, every 20 s) while holding the cell at −65 mV. Following a 4-min stable baseline, various concentrations of test compounds were bath-applied for 16 min. The degree of blockade was quantified as the eEPSC amplitude during the final minute (15–16 min) of drug application, normalized to the baseline.

Western blotting

The mPFC total protein for BDNF and CD73 detection were performed in WT, *Adora1*$^{-/-}$, *Adora2a*$^{-/-}$ and *Nt5e*$^{-/-}$ mice. Animals were anaesthetized with isoflurane, and the mPFC tissue was quickly dissected from the brain and homogenized in lysis RIPA buffer (50 mM Tris HCl, pH 7.4 (Sigma), 150 mM NaCl, 1% Triton X-100 (Sigma) and protease inhibitor cocktail (Sigma)) on ice. After determining the protein concentration with the bicinchoninic acid assay, 35 mg of total protein from each mPFC sample was loaded onto a 4–20% SDS–PAGE gel for separation. Proteins were then transferred to a polyvinylidene fluoride membrane for western blot analyses. Rabbit anti-BDNF (1:1,000; Abcam, ab108319), rabbit anti-CD73 (1:1,000; Cell Signaling Technology, 13160), rabbit anti-GAPDH (1:5,000; Cell Signaling Technology, 2118), rabbit anti-HSP90 (1:1,000; Cell Signaling Technology, 4874) and HRP-conjugated antibody goat anti-rabbit IgG (1:30,000; Sigma-Aldrich, AP156P) were used, along with high-sensitivity ECL reagent (Perkin Elmer). All bands were analysed using ImageJ software.

Histology and immunohistochemistry

For tissue preparation, mice were anaesthetized with an overdose of pentobarbital and intracardially perfused with PBS followed by 4% paraformaldehyde in PBS. Brains were postfixed in 4% paraformaldehyde for 4 h at room temperature or overnight at 4 °C, then cryoprotected in 30% sucrose until they sank. Coronal sections (35 µm) were prepared using a cryostat (Leica CM1950). Virus expression and fibre implantation sites were verified in brain sections using an Olympus VS120 slide scanner with a ×10 objective.

Statistics and reproducibility

All experiments were independently performed ≥3 times with mice randomly assigned to each group, and investigators were blinded to allocation during behavioural experiments and outcome assessment. No statistical methods were used to predetermine the sample sizes.

Reporting summary

Further information on research design is available in the Nature Portfolio Reporting Summary linked to this article.

Data availability

All data supporting the findings of this study are provided within the Article and its Supplementary Information. Any additional information required to reproduce analyses is available from the corresponding authors. Source data are provided with this paper.

51. Lin, R. et al. Directed evolution of adeno-associated virus for efficient gene delivery to microglia. *Nat. Methods* **19**, 976–985 (2022).
52. Yuan, Z. et al. A corticoamygdalar pathway controls reward devaluation and depression using dynamic inhibition code. *Neuron* **111**, 3837–3853 (2023).
53. Li, Y. et al. Hypothalamic circuits for predation and evasion. *Neuron* **97**, 911–924 (2018).
54. Wu, Z. et al. Neuronal activity-induced, equilibrative nucleoside transporter-dependent, somatodendritic adenosine release revealed by a GRAB sensor. *Proc. Natl Acad. Sci. USA* **120**, e2212387120 (2023).
55. Peng, W. et al. Regulation of sleep homeostasis mediator adenosine by basal forebrain glutamatergic neurons. *Science* **369**, eabb0556 (2020).
56. Wu, Z. et al. A sensitive GRAB sensor for detecting extracellular ATP in vitro and in vivo. *Neuron* **110**, 770–782 (2022).
57. Kim, K. S. & Han, P. L. Optimization of chronic stress paradigms using anxiety- and depression-like behavioral parameters. *J. Neurosci. Res.* **83**, 497–507 (2006).
58. Powell, T. R., Fernandes, C. & Schalkwyk, L. C. Depression-related behavioral tests. *Curr. Protoc. Mouse Biol.* **2**, 119–127 (2012).
59. Xin, Q. et al. Neuron–astrocyte coupling in lateral habenula mediates depressive-like behaviors. *Cell* **188**, 3291–3309 (2025).
60. van Buel, E. M. et al. Mouse repeated electroconvulsive seizure (ECS) does not reverse social stress effects but does induce behavioral and hippocampal changes relevant to electroconvulsive therapy (ECT) side-effects in the treatment of depression. *PLoS ONE* **12**, e0184603 (2017).
61. Dai, R. et al. A neuropsin-based optogenetic tool for precise control of G_q signaling. *Sci. China Life Sci.* **65**, 1271–1284 (2022).

Acknowledgements We thank J. Chen for providing *Nt5e*$^{-/-}$ mice; J. Li, X. Han and G. Wang for drug reagents; X. Qi and Y. He for advice on medicinal chemistry; B. Li for advice on statistical analysis; and staff at the Vector Core, Laboratory Animal Resource Center and at the Optical Imaging Core at CIBR for technical support. This study was supported by CAMS Innovation Fund for Medical Sciences (CIFMS 2024-I2M-ZD-012 to M.L.), a China Brain Initiative grant (STI2030-Major Projects 2021ZD0202803 to M.L.), the Research Unit of Medical Neurobiology at the Chinese Academy of Medical Sciences (2019RU003 to M.L.), the New Cornerstone Investigator Program (M.L. and Y.L.), the Beijing Municipal Government (M.L.), the National Key R&D Program of China (2022YFE0108700 to Y.L.), the National Natural Science Foundation of China (32400820 to Z.Y., 32422031 to Z.W., T2350008 to X.W., and 22207103 to H.W.) and the Strategic Priority Research Program of the Chinese Academy of Sciences (XDB0450102 to X.W.).

Author contributions M.L., C.Y. and N.W. conceived the study. C.Y., N.W., Z.Y. and X.F. performed the behavioural assays. C.Y., N.W. and Z.Y. performed fibre photometry. Y.C. and J.Q. conducted early exploration of the project and advised on western blotting. Y.C. and Y.Z. conducted ex vivo electrophysiology. H.Z. and H.W. synthesized the ketamine analogue compounds under X.W.'s supervision. Y.L. and Z.W. provided the $GRAB_{Ado1.0}$, $GRAB_{Ado1.0\text{-}mut}$, $GRAB_{ATP1.0}$ and PercevalHR AAV vectors. H.M. conducted metabolomic analysis; W.G. advised on data interpretation. C.Y. and M.L. analysed the data and wrote the manuscript with input from all authors.

Competing interests M.L. is the scientific founder of ThinkerTech Biotech, GenAns Biotech and Neucyber Neurotech. This relationship did not influence this study. The other authors declare no competing interests.

Additional information

Supplementary information The online version contains supplementary material available at https://doi.org/10.1038/s41586-025-09755-9.

Correspondence and requests for materials should be addressed to Xiaohui Wang or Minmin Luo.

Peer review information *Nature* thanks Susan Masino and the other, anonymous, reviewer(s) for their contribution to the peer review of this work.

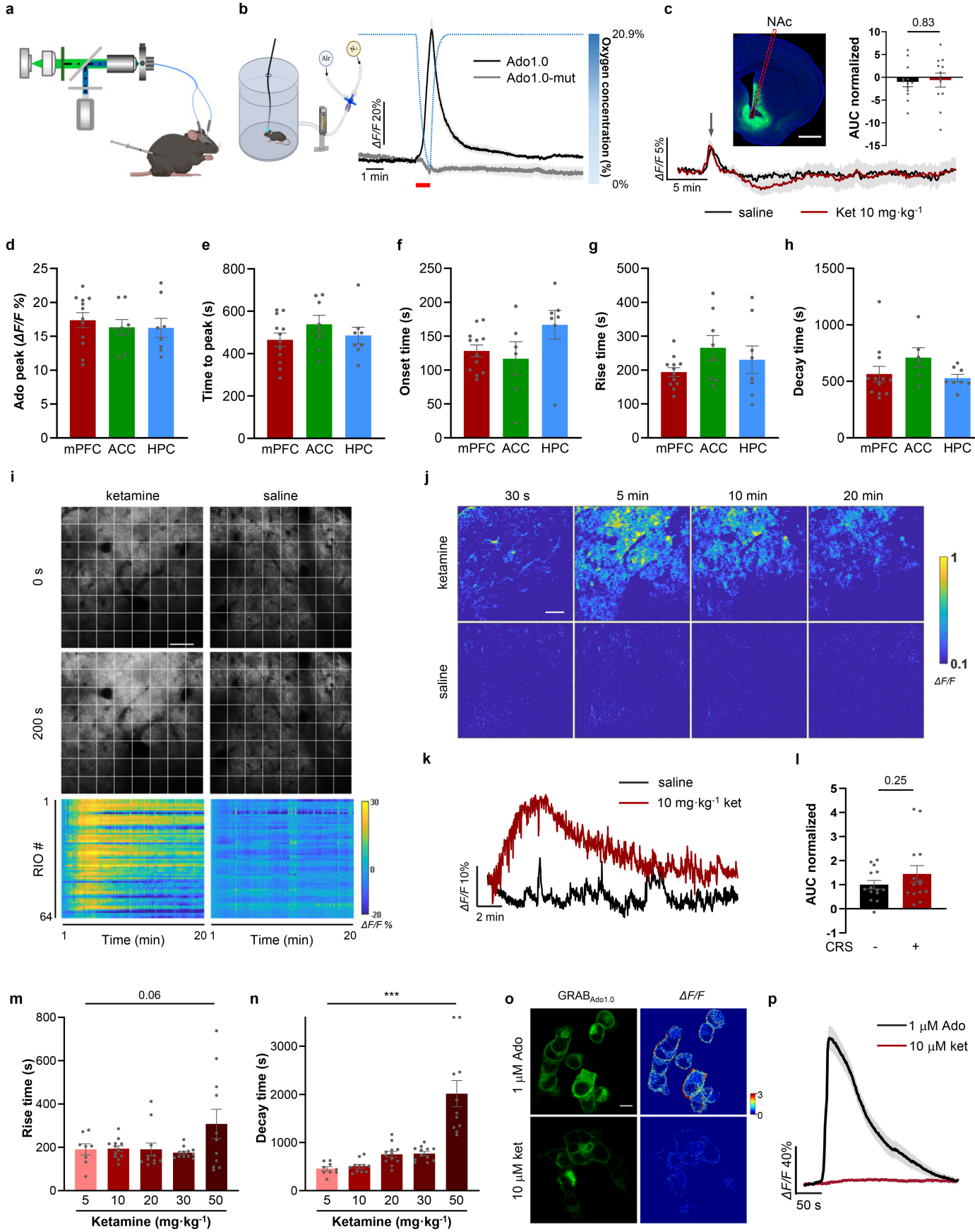

Extended Data Fig. 1 | See next page for caption.

Extended Data Fig. 1 | Characterization and validation of ketamine-induced adenosine signals. a, Schematic of fiber photometry setup for monitoring $GRAB_{Ado1.0}$ signals. **b**, Schematic diagram of acute hypoxia chamber (left) and real-time fluorescence changes of $GRAB_{Ado1.0}$ and $GRAB_{Ado1.0\text{-}mut}$ probes in the mPFC during acute hypoxia (right; red line). Blue dashed line represents oxygen levels. **c**, Adenosine signals were not detected in the nucleus accumbens (NAc) following ketamine administration (10 mg·kg^{-1}, i.p.) compared to saline control. Scale bar, 1 mm. **d**-**h**, Quantification of $GRAB_{Ado1.0}$ signals induced by ketamine (10 mg·kg^{-1}, i.p.) in the mPFC, ACC, and HPC, showing adenosine peak amplitude (d), average time to peak (**e**), onset time (**f**), rise time (**g**), and decay time (**h**). **i**, Two-photon images show fluorescence changes of the $GRAB_{Ado1.0}$ probe in the prefrontal cortex at 0 s (top) and 200 s (middle) following ketamine and saline administration. Bottom, corresponding time-course heatmaps for each region of interest (ROI). Scale bar, 50 μm. **j**, Heatmaps showing extracellular adenosine changes in the cortex at different time points after ketamine and saline administration. Scale bar, 50 μm. **k**, Time course of mean adenosine levels in prefrontal cortex ROIs following ketamine or saline administration. **l**, Area under the curve (AUC) of adenosine levels in the mPFC of CRS and naive mice after ketamine administration (10 mg·kg^{-1}, i.p.), normalized to the naive group. **m**, **n**, Rise time (**m**) and decay time (**n**) of $GRAB_{Ado1.0}$ signals in the mPFC in response to different ketamine doses. **o**, **p**, Specificity of the $GRAB_{Ado1.0}$ probe validated in cultured HEK293T cells. **o**, Heatmaps and **p**, time course of fluorescence changes following application of adenosine and ketamine (n = 15 cells per group). Scale bar, 10 μm. Data are mean ± s.e.m. (shading in **b**, **c**, **p**; error bars in **d**-**h**, **l**-**n**). Statistical analyses used a two-tailed unpaired t-test (**c**, **l**) and one-way ANOVA (**m**, **n**) (***$P < 0.001$). See Supplementary Table 1 for detailed statistics. The schematics in **a** and **b** were created using BioRender (https://www.biorender.com).

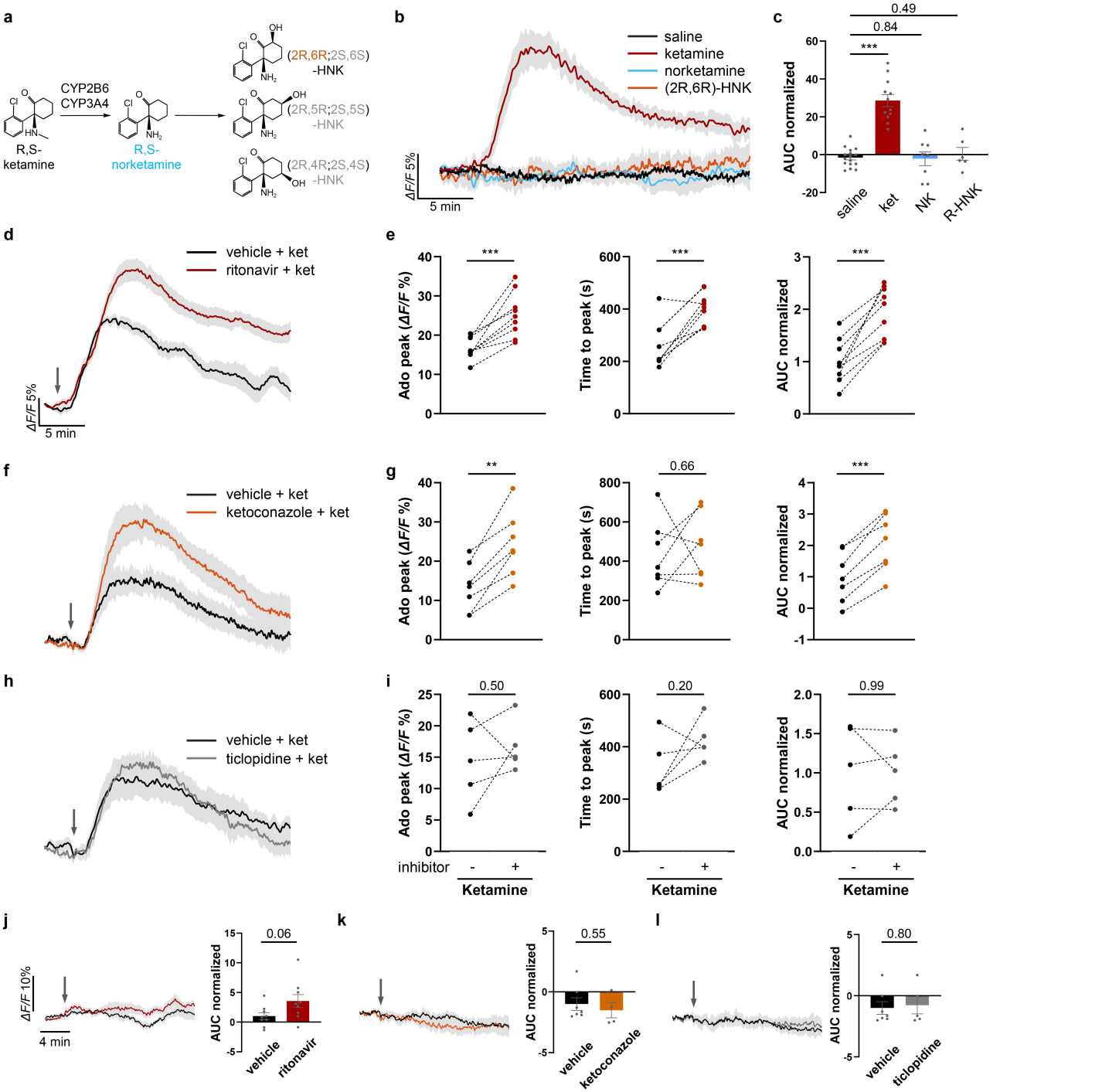

Extended Data Fig. 2 | Effect of ketamine metabolites and metabolism inhibitors on adenosine release in the mPFC. a, Schematic of ketamine metabolism pathways. **b**, **c**, Time course of extracellular adenosine levels in the mPFC (b) and and corresponding AUC (**c**) following administration of ketamine, norketamine (NK), (2 R,6 R)-HNK (all at 10 mg·kg^{-1}, i.p.), or saline. Area under the curve (AUC, normalized to saline) (**c**) was calculated post-administration. **d**, **e**, Effect of ritonavir pretreatment (50 mg·kg^{-1}, i.p.) on ketamine-induced adenosine release. d, Adenosine time course with and without ritonavir. e, Quantification of adenosine peak (*ΔF/F* %), time to peak, and AUC (normalized to vehicle). Recordings were performed on separate days in the same cohort of mice. **f**, **g**, Effect of ketoconazole pretreatment (50 mg·kg^{-1}, i.p.) on ketamine-induced adenosine signals. Same conventions as in (**d**, **e**). **h**, **i**, Effects of ticlopidine pretreatment (20 mg·kg^{-1}, i.p.) on ketamine-induced adenosine signals, displayed as in **d**, **e**. **j**-**l**, Time course and AUC of extracellular adenosine in the mPFC after administration of ritonavir (**j**), ketoconazole (**k**), or ticlopidine (**l**) alone, compared to vehicle. Data are mean ± s.e.m. (shading in **b, d, f, h, j**-**l**; error bars in **c, j**-**l**). Statistical analyses used a two-tailed paired t-test (**e, g, i**) and two-tailed unpaired t-tests (**c, j**-**l**) (**P < 0.01, ***P < 0.001). See Supplementary Table 1 for detailed statistics.

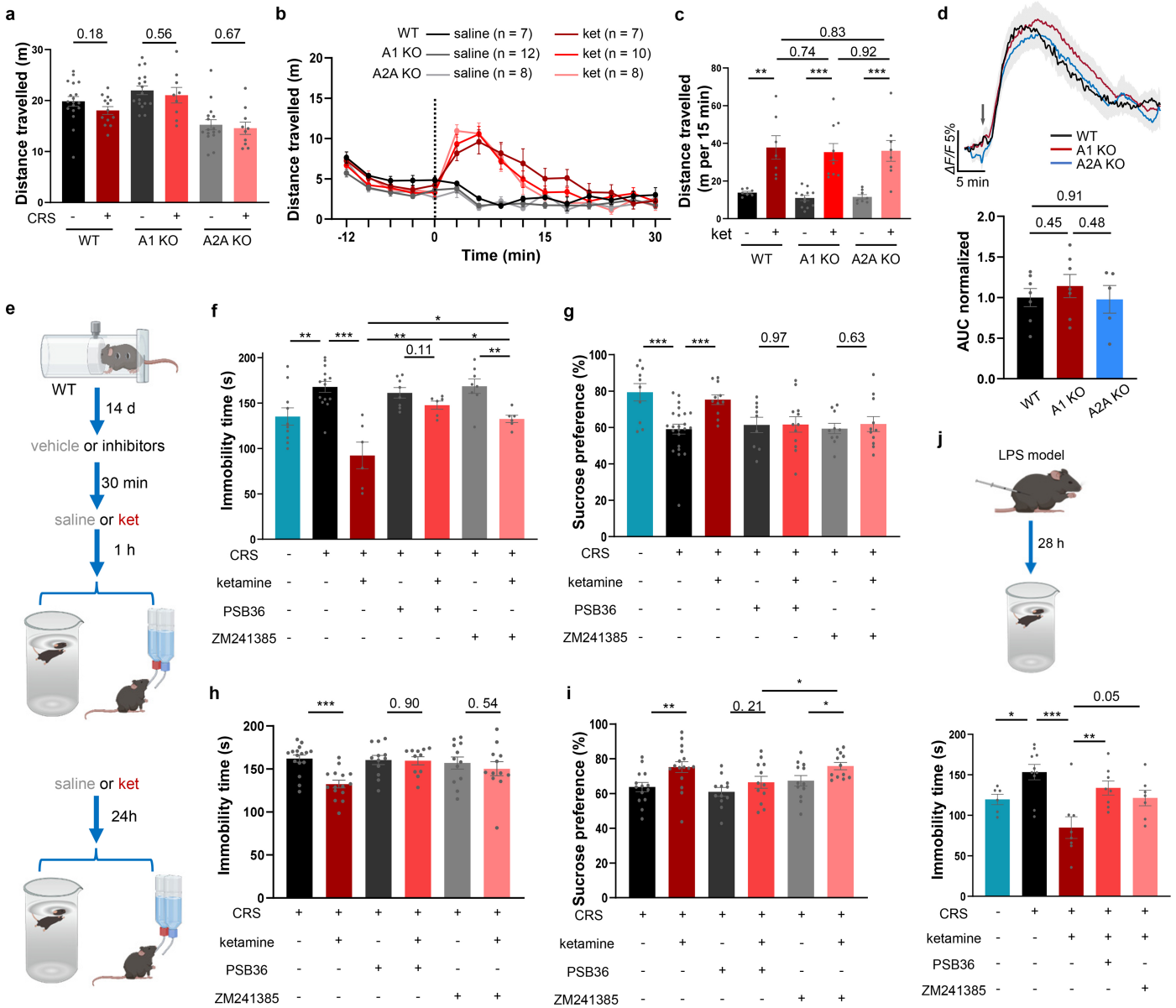

Extended Data Fig. 3 | Adenosine receptor activity is critical for ketamine's antidepressant effects without altering locomotion or adenosine release. **a**, Total distance traveled in the open-field test for WT, A1KO and A2A KO mice. **b**, **c**, Time-course (**b**) and quantification (**c**) of locomotor activity in WT, A1KO and A2A KO mice following ketamine (10 mg·kg^{-1}, i.p.) and saline administration. Mouse sample sizes (n) are shown in **b**. **d**, Time course of extracellular adenosine levels in the mPFC of WT, A1KO and A2A KO mice after equal dose of ketamine, quantification of area under the curve (AUC, normalized to WT). **e**, Experimental timeline for assessing the impact of adenosine receptor antagonists on the antidepressant effects of ketamine. **f**-**i**. Effects of pretreatment with adenosine receptor antagonists (PSB36 for A1 and ZM241385 for A2A; 1 mg·kg^{-1}, i.p.) on ketamine's antidepressant actions (forced swimming immobility: **f**, **h**; sucrose preference: **g**, **i**) 1 h (**f**, **g**) and 24 h (**h**, **i**) after ketamine administration. **j**, upper, Experimental timeline for testing the effect of adenosine receptor antagonists on the antidepressant-like action of ketamine in a lipopolysaccharide (LPS)-induced depression model. lower, Effects of pretreating an A1 antagonist (PSB36, 1 mg·kg^{-1}, i.p.) and A2A antagonist (ZM241385, 1 mg·kg^{-1}, i.p.) on ketamine's antidepressant actions in a FST test of LPS-challenged mice. Data are mean ± s.e.m. (error bars in **a**–**c**, **f**-**j**; shading in **d**). Two-tailed unpaired t-tests were used for **a**, **c**, **d**, **f**-**j** (*P < 0.05, **P < 0.01, ***P < 0.001). See Supplementary Table 1 for detailed statistics. The schematics in **e** and **j** were created using BioRender (https://www.biorender.com).

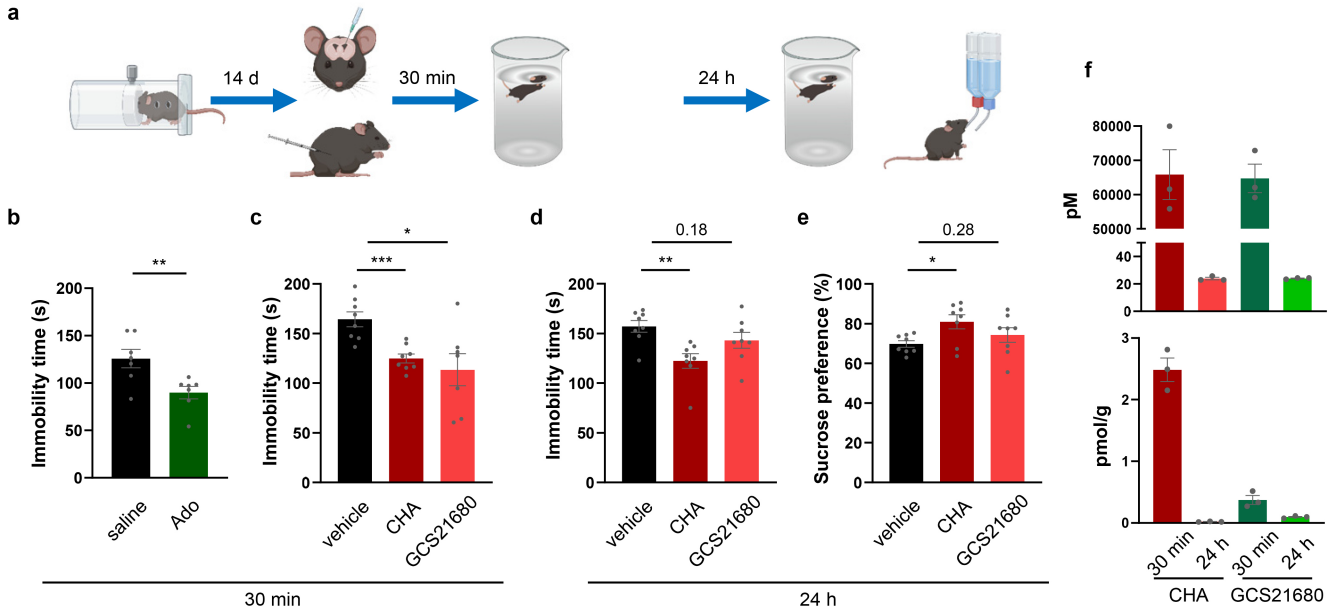

Extended Data Fig. 4 | Adenosine receptor activation produces antidepressant-like effects. a, Experimental timelines for assessing the antidepressant-like effects of direct adenosine administration or systemic delivery of specific adenosine receptor agonists in mice subjected to chronic restraint stress (CRS). **b**, **c**, Rapid antidepressant-like effects. **b**, Immobility time in the FST 30 min after intracerebroventricular (i.c.v.) injection of adenosine (1 µg per mouse). **c**, Immobility time in the FST 30 min after intraperitoneal (i.p.) injection of an A1 receptor agonist (CHA; 0.1 mg·kg^{-1}) or an A2A receptor agonist (CGS21680; 0.1 mg·kg^{-1}). **d**, **e**, Sustained antidepressant-like effects. Immobility time in the FST (**d**) and sucrose preference (**e**) were measured 24 h after i.p. administration of CHA or CGS21680 in CRS mice. **f**, Concentrations of CHA and CGS21680 in serum (top) and brain tissue (bottom) at 30 min and 24 h after i.p. injection, measured by LC-MS. Data are mean ± s.e.m. (error bars in **b**–**f**). Two-tailed unpaired t-tests were used for **b**–**e** (*P < 0.05, **P < 0.01, ***P < 0.001). See Supplementary Table 1 for detailed statistics. The schematic in **a** was created using BioRender (https://www.biorender.com).

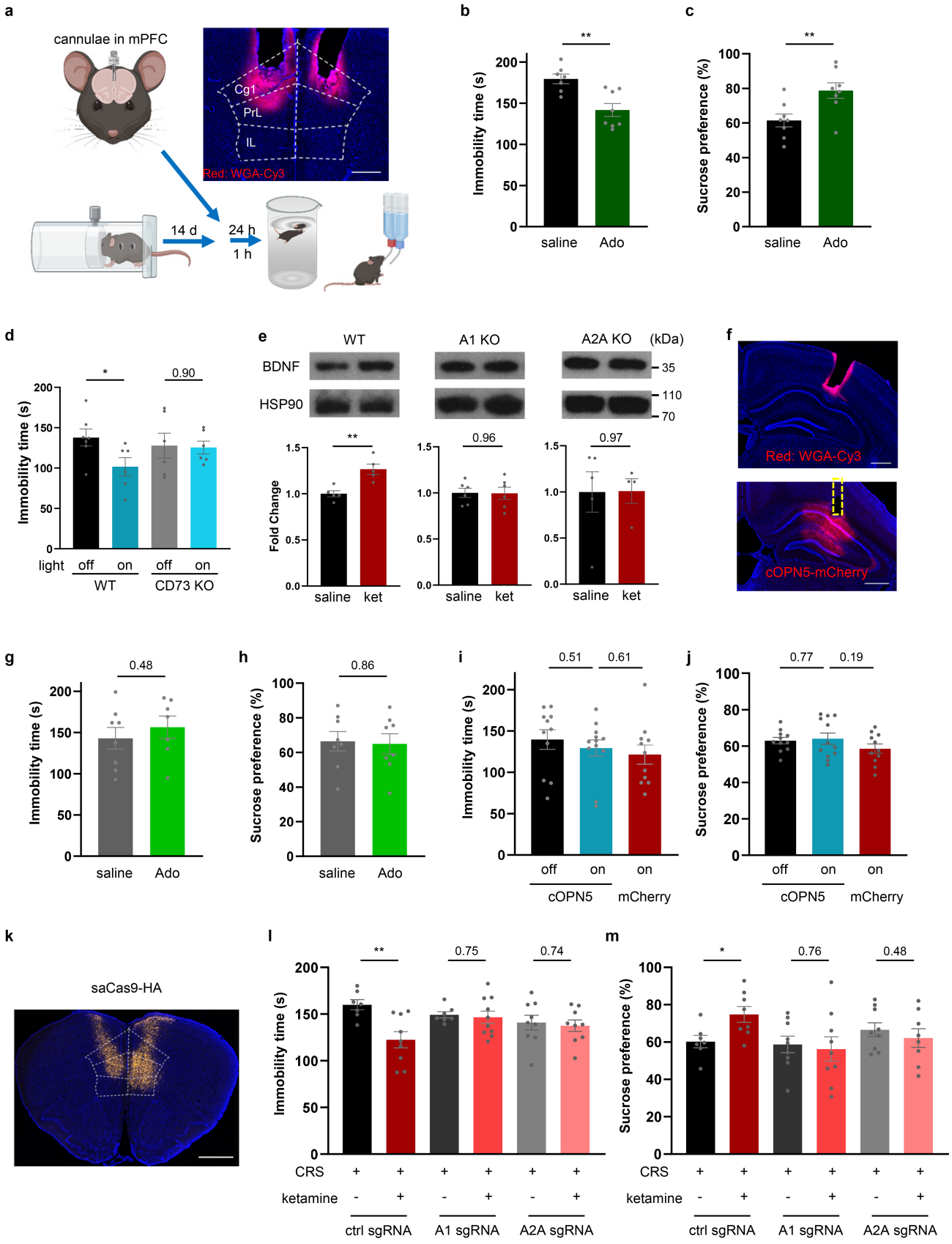

Extended Data Fig. 5 | See next page for caption.

Extended Data Fig. 5 | Regional specificity of adenosine-mediated effects. **a-c**, Direct infusion of adenosine into the mPFC produced sustained antidepressant-like effects. **a**, Experimental timeline and representative image of the bilateral infusion site in the mPFC of CRS. Scale bar, 500 µm. **b**,**c**, Immobility time in the forced swim test (FST; **b**) and sucrose preference (**c**) were measured 24 h after infusion of adenosine (0.1 µg per side). **d**, FST immobility time in CRS-exposed WT and CD73 knockout (KO) mice following cOpn5-mediated optogenetic stimulation in the mPFC. **e**, Ketamine-induced BDNF upregulation in the mPFC requires A1/A2A receptor signaling. Top, representative western blots. Bottom, quantified BDNF protein in WT, A1 KO and A2A KO mice 30 min after receiving saline or ketamine (10 mg·kg^{-1}, i.p.). **f-j**, Adenosine signaling in the dorsal HPC (dHPC) does not elicit antidepressant-like effects. **f**, images showing adenosine infusion (upper) and optogenetically induced adenosine production (lower) within the dHPC. Scale bar, 500 µm. **g**, **h**, FST immobility (**g**) and sucrose preference (**h**) in CRS mice 24 h post-infusion (0.1 µg per side). **i**, **j**, FST immobility (**i**) and sucrose preference (**j**) measured 1 h post-stimulation (cOpn5 vs mCherry) in CRS mice. **k-m**, Adenosine receptor signaling in the mPFC is necessary for the rapid antidepressant-like effects of ketamine. **k**, Representative image of saCas9-HA expression (yellow) in the mPFC. Scale bar, 1 mm. **l**, **m**, Immobility time in the FST (**l**) and sucrose preference (**m**) were measured 1 h after ketamine administration (10 mg·kg^{-1}, i.p.) in CRS-exposed Cas9 mice expressing sgRNAs targeting the A1 receptor, the A2A receptor or a non-targeting control. Data are mean ± s.e.m. (error bars in **b**–**e, g**–**j, l, m**). Two-tailed unpaired t-tests were used for **b**–**e, g**–**j, l, m** (*P < 0.05, **P < 0.01). See Supplementary Table 1 for detailed statistics. The schematic in **a** was created using BioRender (https://www.biorender.com).

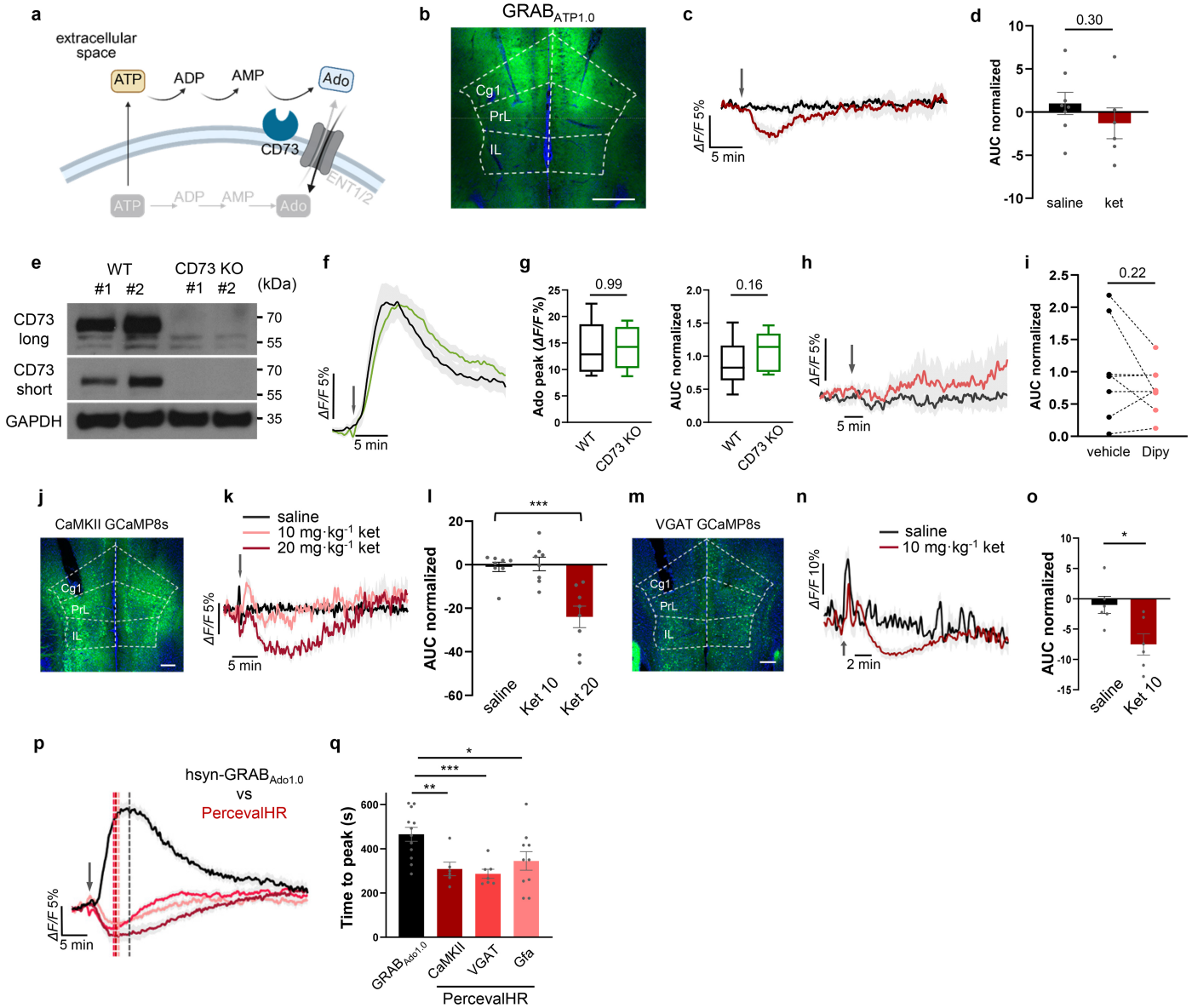

Extended Data Fig. 6 | Ketamine-induced adenosine surges are independent of extracellular ATP hydrolysis and broad neuronal hyperactivation. a, Schematic of extracellular adenosine generation via ATP hydrolysis. **b-d**, Ketamine does not alter extracellular ATP levels in the mPFC. **b**, Representative image of GRAB$_{ATP1.0}$ expression (green). Scale bar, 500 µm. **c**, Time course of extracellular ATP following ketamine (10 mg·kg^{-1}, i.p.) or saline administration. **d**, Corresponding AUC, normalized to saline. **e-g**, Ketamine-induced adenosine release does not depend on the ectonucleotidase CD73. **e**, Western blot validation of CD73 knockout (KO). **f**, Time course of extracellular adenosine in WT (n = 13 mice) and CD73 KO mice (n = 10 mice) after ketamine administration. **g**, Quantification of adenosine peak and AUC, normalized to WT. **h**, **i**, Time course (**h**) and AUC (**i**) of extracellular adenosine in the mPFC following the administration of dipyridamole (i.c.v., 1 µg) or vehicle. **j-l**, Ketamine inhibited Ca^{2+} signaling in pyramidal neurons. **j**, Representative images show GCaMP8s expression (green) in mPFC pyramidal neurons of CaMKII-Cre mice. **k**, Time course of Ca^{2+} signals in mPFC pyramidal neurons in response to ketamine (10 and 20 mg·kg^{-1}, i.p.) and saline. **l**, AUC (normalized to saline) quantification of Ca^{2+} signals in pyramidal neurons. Scale bar, 200 µm. **m-o**, Ketamine inhibited Ca^{2+} signaling in inhibitory interneurons. **m**, Representative images showing GCaMP8s expression in GABAergic neurons of VGAT-Cre mice. **n**, Time course of Ca^{2+} signals in mPFC GABAergic neurons in response to ketamine (10 mg·kg^{-1}, i.p.) and saline. **o**, AUC quantification of Ca^{2+} signals in GABAergic neurons. Scale bar, 200 µm. **p**, **q**, Temporal dynamics of intracellular energy and extracellular adenosine. **p**, Aligned time courses of PercevalHR (ATP/ADP) and GRAB$_{Ado1.0}$ (adenosine) signals following ketamine injection (10 mg·kg^{-1}; adenosine data replotted from Fig. 1e). **q**, Quantification of the time to peak for each signal. Data are mean ± s.e.m. (shading in **c, f, h, k, n, p**; error bars in **d, g, i, l, o, q**). The box plot in **g** shows the median (center line), first and third quartiles (box bounds), and 1.5 × IQR (whiskers). Statistical analyses used a two-tailed paired t-test (i) and two-tailed unpaired t-tests (**d, g, l, o, q**) (*P < 0.05, **P < 0.01, ***P < 0.001). See Supplementary Table 1 for detailed statistics. The schematic in **a** was created using BioRender (https://www.biorender.com).

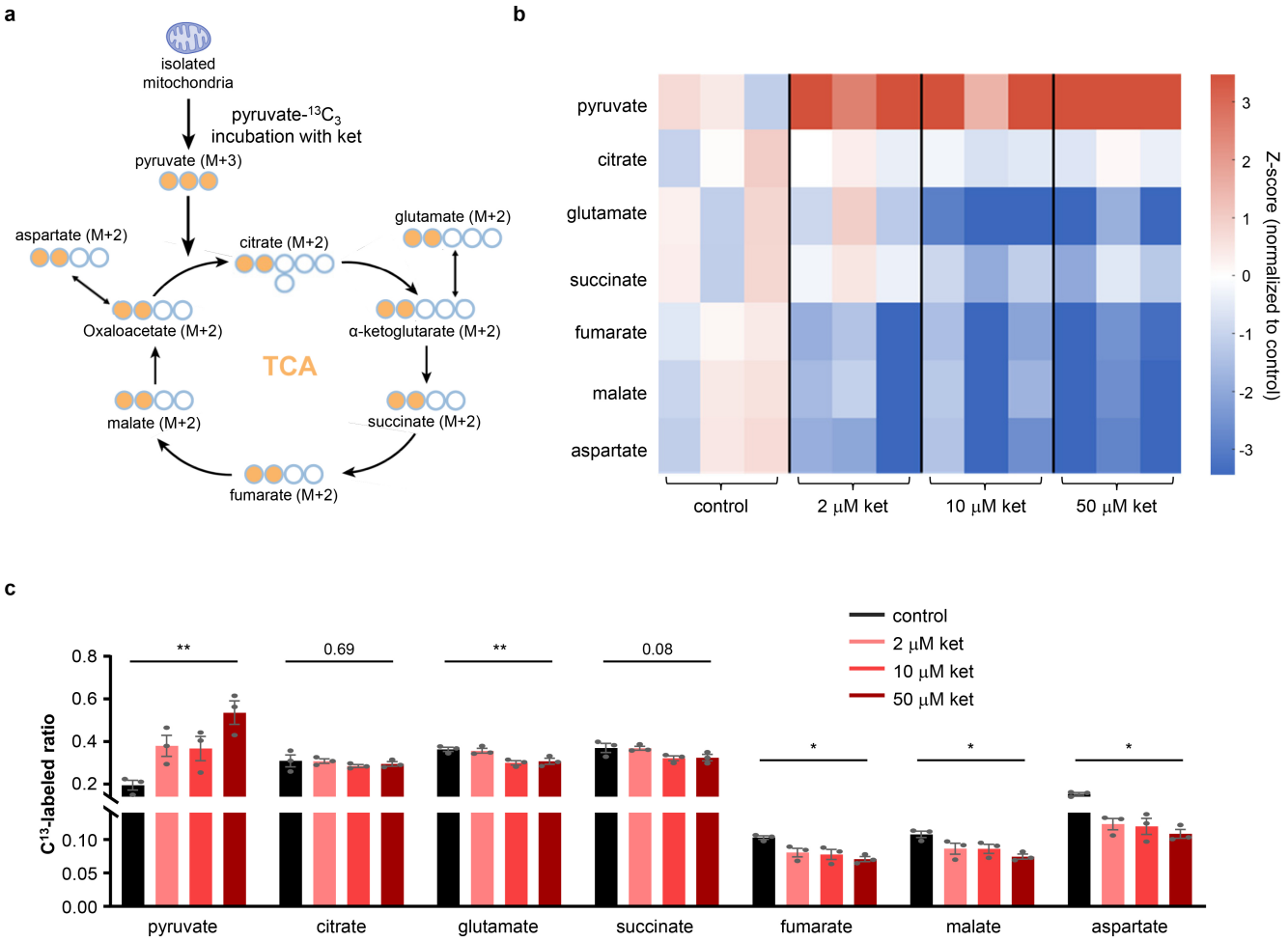

Extended Data Fig. 7 | Ketamine directly modulates mitochondrial TCA cycle flux. a, Schematic illustrating the incorporation of ^{13}C atoms from pyruvate-$^{13}C_3$ into key tricarboxylic acid (TCA) cycle intermediates. **b**, Heatmap showing the relative ^{13}C-enrichment of TCA cycle metabolites in isolated brain mitochondria incubated with increasing concentrations of ketamine (3 replicates for each concentration). Data are Z-score normalized to the vehicle control group for each metabolite. **c**, Quantification of ^{13}C-labeling for representative TCA cycle intermediates across ketamine concentrations. Data are mean ± s.e.m. (error bars in **c**). One-way ANOVA was used (*$P < 0.05$, **$P < 0.01$). See Supplementary Table 1 for detailed statistics.

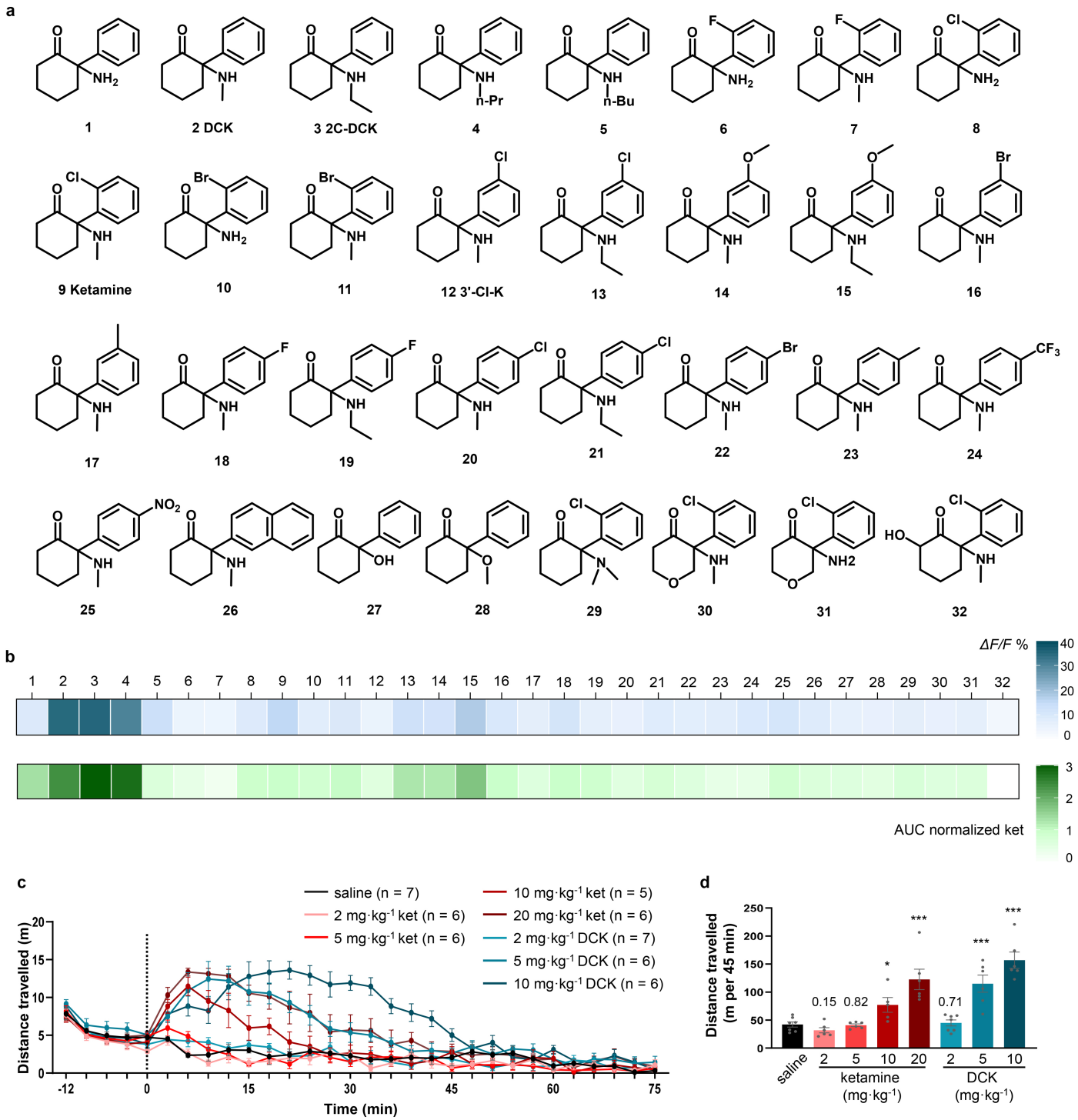

Extended Data Fig. 8 | In vivo characterization of ketamine analogues: adenosine release and locomotor activity. a, Chemical structures of the synthesized ketamine analogues. **b**, Heatmap of peak adenosine signal (upper) and AUC (lower) in the mPFC following administration of each analogue (10 mg·kg^{-1}, i.p.). All values are normalized to the response induced by an equivalent dose of ketamine. **c**, Locomotor activity time course after ketamine or DCK administration. Baseline recorded for 15 min; i.p. injection at dashed line; activity monitored for 75 min post-injection. Mouse sample sizes (n) are shown near the data series. **d**, Dose-dependent increase in locomotor activity induced by ketamine and DCK. Data are mean ± s.e.m. (**c**, **d**). Two-tailed unpaired *t*-tests between drugs and saline control (*P < 0.05, ***P < 0.001). See Supplementary Table 1 for detailed statistics.

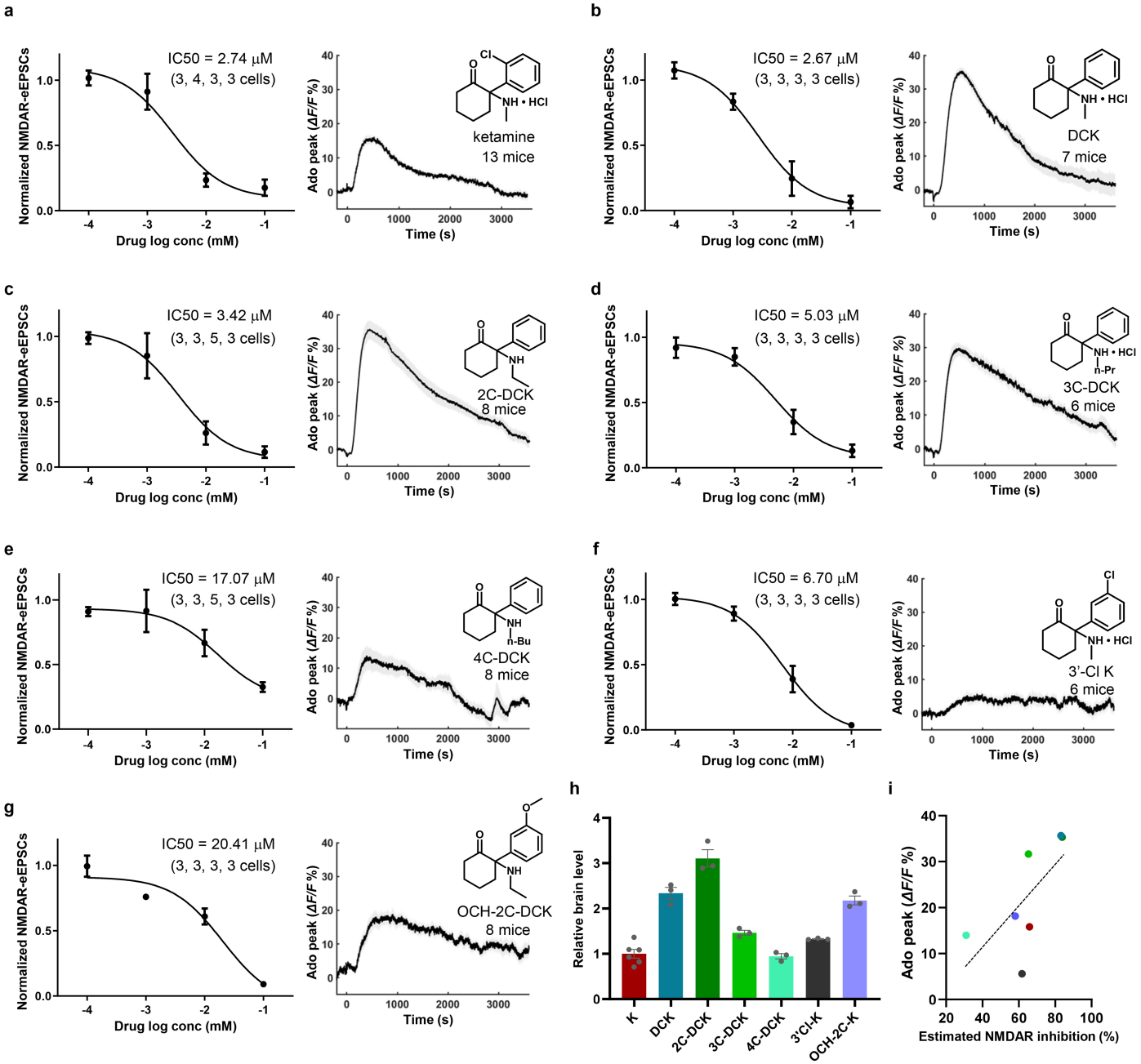

Extended Data Fig. 9 | Comparative analysis of NMDA receptor blockade and adenosine modulation by ketamine analogues. **a**–**g**, Normalized NMDA receptor-mediated excitatory postsynaptic currents (NMDAR-eEPSCs; left) and adenosine responses (right) for each analogue. The numbers in the left panels indicate the sample size (n, cells) for each concentration (increasing left to right). Those in the right panels indicate mouse sample size. **h**, Relative brain tissue concentrations of ketamine analogues (n = 6, 3, 3, 3, 3, 3 mice, respectively) 10 min after intraperitoneal injection (i.p.), measured by LC–MS and normalized to ketamine. **i**, Lack of significant correlation between estimated NMDAR inhibition in brain tissue and adenosine modulation in the mPFC by ketamine analogues (Pearson correlation, $P = 0.097$). Data are mean ± s.e.m. (error bars in **a**–**h**; shading in **a**–**g**). See Supplementary Table 1 for detailed statistics.

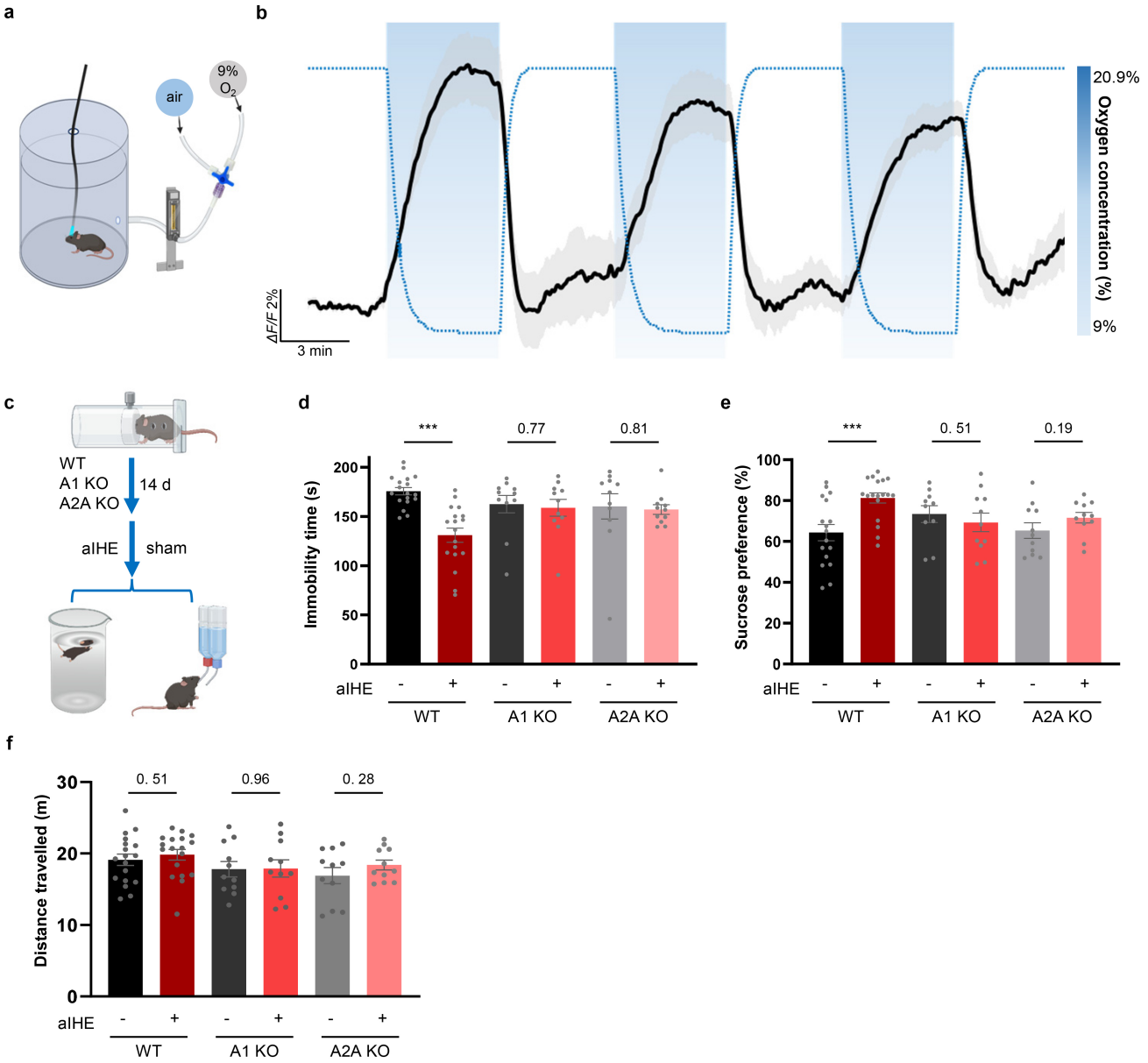

Extended Data Fig. 10 | Acute intermittent hypoxia (aIH) alleviates depressive-like phenotypes through adenosine signaling. a, Experimental timeline for acute intermittent hypoxia (aIH) exposure in mice. **b**, Oxygen-dependent adenosine dynamics in the mPFC, monitored with GRABAdo1.0 sensor during graded hypoxia (9–21% O_2; n = 11 mice). **c**-**e**, Experimental paradigm for assessing aIH antidepressant efficacy (**c**), FST immobility time (**d**), and sucrose preference (**e**) of CRS-challenged WT, A1 KO and A2A KO mice. **f**, Open-field locomotor activity in WT, adenosine receptor A1 KO and A2A KO mice before and after aIH following CRS. Data are mean ± s.e.m. (shading in **b**; error bars in **d**–**f**). Two-tailed unpaired t-tests were used for **d**–**f** (***$P < 0.001$). See Supplementary Table 1 for detailed statistics. The schematics in **a** and **c** were created using BioRender (https://www.biorender.com).

nature portfolio

Corresponding author(s): Minmin Luo

Last updated by author(s): Oct 14, 2025

Reporting Summary

Nature Portfolio wishes to improve the reproducibility of the work that we publish. This form provides structure for consistency and transparency in reporting. For further information on Nature Portfolio policies, see our Editorial Policies and the Editorial Policy Checklist.

Statistics

For all statistical analyses, confirm that the following items are present in the figure legend, table legend, main text, or Methods section.

n/a	Confirmed
☐	☒ The exact sample size (*n*) for each experimental group/condition, given as a discrete number and unit of measurement
☐	☒ A statement on whether measurements were taken from distinct samples or whether the same sample was measured repeatedly
☐	☒ The statistical test(s) used AND whether they are one- or two-sided *Only common tests should be described solely by name; describe more complex techniques in the Methods section.*
☒	☐ A description of all covariates tested
☒	☐ A description of any assumptions or corrections, such as tests of normality and adjustment for multiple comparisons
☐	☒ A full description of the statistical parameters including central tendency (e.g. means) or other basic estimates (e.g. regression coefficient) AND variation (e.g. standard deviation) or associated estimates of uncertainty (e.g. confidence intervals)
☐	☒ For null hypothesis testing, the test statistic (e.g. *F*, *t*, *r*) with confidence intervals, effect sizes, degrees of freedom and *P* value noted *Give P values as exact values whenever suitable.*
☒	☐ For Bayesian analysis, information on the choice of priors and Markov chain Monte Carlo settings
☒	☐ For hierarchical and complex designs, identification of the appropriate level for tests and full reporting of outcomes
☒	☐ Estimates of effect sizes (e.g. Cohen's *d*, Pearson's *r*), indicating how they were calculated

Our web collection on statistics for biologists contains articles on many of the points above.

Software and code

Policy information about availability of computer code

Data collection	In vivo two-photon imaging was performed using a STELLARIS 8 DIVE Multiphoton Microscope (Leica) equipped with a 25× water-immersion objective (NA 1.05). Brain slice images were acquired with an Olympus VS120 slide scanner using a 10× objective. Whole-cell patch-clamp recordings were obtained using a MultiClamp 700B amplifier (Molecular Devices, USA), with signals digitized at 20 kHz and low-pass filtered at 2 kHz. HEK293T live-cell imaging was conducted on a Zeiss LSM 880 inverted confocal microscope (Carl Zeiss AG) with a 20×/0.8 NA Plan-Apochromat objective. Fiber photometry recordings were obtained using a multichannel fiber photometry system (ThinkerTech, Nanjing, China) and an independent two-color multichannel optical fiber photometry setup (Optical Imaging Facility, CIBR). Behavioral tracking was performed using the native Windows 10 camera application alongside an infrared open-field arena (Med Associates Inc.; 50 × 50 × 30 cm). Drug concentrations were then quantified using a SCIEX 7500 triple quadrupole mass spectrometer. Mitochondria metabolite profiling was performed using hydrophilic interaction chromatography (HILIC) on an XBridge BEH Amide column (Waters) coupled to a Q Exactive PLUS Orbitrap mass spectrometer (Thermo Fisher Scientific).
Data analysis	Image processing and quantification were performed using ImageJ (FIJI distribution, version 2.14.0). Fiber photometry signals were analyzed with a custom MATLAB script (version 2022a, MathWorks, USA; provided by ThinkerTech, Nanjing, China). Behavioral parameters were quantified using Activity Monitor software (version 7, Med Associates Inc.). Metabolite identification, quantification, and isotopic tracing analyses were carried out using El-MAVEN software. Statistical analyses were conducted with GraphPad Prism (version 9, GraphPad Software, USA).

For manuscripts utilizing custom algorithms or software that are central to the research but not yet described in published literature, software must be made available to editors and reviewers. We strongly encourage code deposition in a community repository (e.g. GitHub). See the Nature Portfolio guidelines for submitting code & software for further information.

Data

Policy information about availability of data

All manuscripts must include a data availability statement. This statement should provide the following information, where applicable:

- Accession codes, unique identifiers, or web links for publicly available datasets
- A description of any restrictions on data availability
- For clinical datasets or third party data, please ensure that the statement adheres to our policy

There are no restrictions on data availability in the manuscript. All data supporting the findings of this study are provided within the Article and its Supplementary Information. Source Data files are provided with this paper. Any additional information required to reproduce the analyses is available from the corresponding authors.

Research involving human participants, their data, or biological material

Policy information about studies with human participants or human data. See also policy information about sex, gender (identity/presentation), and sexual orientation and race, ethnicity and racism.

Reporting on sex and gender	N/A
Reporting on race, ethnicity, or other socially relevant groupings	N/A
Population characteristics	N/A
Recruitment	N/A
Ethics oversight	N/A

Note that full information on the approval of the study protocol must also be provided in the manuscript.

Field-specific reporting

Please select the one below that is the best fit for your research. If you are not sure, read the appropriate sections before making your selection.

☒ Life sciences ☐ Behavioural & social sciences ☐ Ecological, evolutionary & environmental sciences

For a reference copy of the document with all sections, see nature.com/documents/nr-reporting-summary-flat.pdf

Life sciences study design

All studies must disclose on these points even when the disclosure is negative.

Sample size	No formal statistical methods were used for a priori sample size determination. Instead, sample sizes were chosen based on the observed variability in analogous experimental assays, including data from our previous studies of similar design (PMID: 38632402) and established protocols in the field (PMID: 27144355; PMID: 29446381).
Data exclusions	In the behavioral experiments, no data from mice that completed tests were excluded from the analysis.
Replication	Each data in this manuscript is reliably reproducible. The replication numbers of each test is at least 3, and have been indicated in the legend of corresponding figures.
Randomization	Animals or cells are randomly assigned into experimental or controls groups.
Blinding	Investigators are blinded to the group allocation before behavior tests.

Behavioural & social sciences study design

All studies must disclose on these points even when the disclosure is negative.

Study description	*Briefly describe the study type including whether data are quantitative, qualitative, or mixed-methods (e.g. qualitative cross-sectional, quantitative experimental, mixed-methods case study).*
Research sample	*State the research sample (e.g. Harvard university undergraduates, villagers in rural India) and provide relevant demographic*

Research sample	*information (e.g. age, sex) and indicate whether the sample is representative. Provide a rationale for the study sample chosen. For studies involving existing datasets, please describe the dataset and source.*
Sampling strategy	*Describe the sampling procedure (e.g. random, snowball, stratified, convenience). Describe the statistical methods that were used to predetermine sample size OR if no sample-size calculation was performed, describe how sample sizes were chosen and provide a rationale for why these sample sizes are sufficient. For qualitative data, please indicate whether data saturation was considered, and what criteria were used to decide that no further sampling was needed.*
Data collection	*Provide details about the data collection procedure, including the instruments or devices used to record the data (e.g. pen and paper, computer, eye tracker, video or audio equipment) whether anyone was present besides the participant(s) and the researcher, and whether the researcher was blind to experimental condition and/or the study hypothesis during data collection.*
Timing	*Indicate the start and stop dates of data collection. If there is a gap between collection periods, state the dates for each sample cohort.*
Data exclusions	*If no data were excluded from the analyses, state so OR if data were excluded, provide the exact number of exclusions and the rationale behind them, indicating whether exclusion criteria were pre-established.*
Non-participation	*State how many participants dropped out/declined participation and the reason(s) given OR provide response rate OR state that no participants dropped out/declined participation.*
Randomization	*If participants were not allocated into experimental groups, state so OR describe how participants were allocated to groups, and if allocation was not random, describe how covariates were controlled.*

Ecological, evolutionary & environmental sciences study design

All studies must disclose on these points even when the disclosure is negative.

Study description	*Briefly describe the study. For quantitative data include treatment factors and interactions, design structure (e.g. factorial, nested, hierarchical), nature and number of experimental units and replicates.*
Research sample	*Describe the research sample (e.g. a group of tagged Passer domesticus, all Stenocereus thurberi within Organ Pipe Cactus National Monument), and provide a rationale for the sample choice. When relevant, describe the organism taxa, source, sex, age range and any manipulations. State what population the sample is meant to represent when applicable. For studies involving existing datasets, describe the data and its source.*
Sampling strategy	*Note the sampling procedure. Describe the statistical methods that were used to predetermine sample size OR if no sample-size calculation was performed, describe how sample sizes were chosen and provide a rationale for why these sample sizes are sufficient.*
Data collection	*Describe the data collection procedure, including who recorded the data and how.*
Timing and spatial scale	*Indicate the start and stop dates of data collection, noting the frequency and periodicity of sampling and providing a rationale for these choices. If there is a gap between collection periods, state the dates for each sample cohort. Specify the spatial scale from which the data are taken*
Data exclusions	*If no data were excluded from the analyses, state so OR if data were excluded, describe the exclusions and the rationale behind them, indicating whether exclusion criteria were pre-established.*
Reproducibility	*Describe the measures taken to verify the reproducibility of experimental findings. For each experiment, note whether any attempts to repeat the experiment failed OR state that all attempts to repeat the experiment were successful.*
Randomization	*Describe how samples/organisms/participants were allocated into groups. If allocation was not random, describe how covariates were controlled. If this is not relevant to your study, explain why.*
Blinding	*Describe the extent of blinding used during data acquisition and analysis. If blinding was not possible, describe why OR explain why blinding was not relevant to your study.*

Did the study involve field work? ☐ Yes ☐ No

Field work, collection and transport

Field conditions	*Describe the study conditions for field work, providing relevant parameters (e.g. temperature, rainfall).*
Location	*State the location of the sampling or experiment, providing relevant parameters (e.g. latitude and longitude, elevation, water depth).*
Access & import/export	*Describe the efforts you have made to access habitats and to collect and import/export your samples in a responsible manner and in compliance with local, national and international laws, noting any permits that were obtained (give the name of the issuing authority, the date of issue, and any identifying information).*

Disturbance | *Describe any disturbance caused by the study and how it was minimized.*

Reporting for specific materials, systems and methods

We require information from authors about some types of materials, experimental systems and methods used in many studies. Here, indicate whether each material, system or method listed is relevant to your study. If you are not sure if a list item applies to your research, read the appropriate section before selecting a response.

Materials & experimental systems

n/a	Involved in the study
☐	☒ Antibodies
☐	☒ Eukaryotic cell lines
☒	☐ Palaeontology and archaeology
☐	☒ Animals and other organisms
☒	☐ Clinical data
☒	☐ Dual use research of concern
☒	☐ Plants

Methods

n/a	Involved in the study
☒	☐ ChIP-seq
☒	☐ Flow cytometry
☒	☐ MRI-based neuroimaging

Antibodies

Antibodies used: Primary antibody including: Rabbit anti-BDNF (1:1000; Abcam, #ab108319), rabbit anti-CD73 (1:1000; Cell Signaling Technology, #13160), rabbit anti-GAPDH (1:5000; Cell Signaling Technology, #2118) and rabbit anti-HSP90 (1:1000; Cell Signaling Technology, #4874). Secondary antibody including: Goat Anti-Rabbit IgG Antibody, Fc, HRP conjugate (1:30000, Sigma-Aldrich, AP156P).

Validation: All primary antibodies were validated by either the manufacturer or our in-house tests using knockout mice. Specifically, rabbit anti-CD73 (Cell Signaling Technology, #13160) was confirmed using CD73 KO mice in both our study and by the manufacturer; rabbit anti-BDNF (Abcam, #ab108319), anti-GAPDH (Cell Signaling Technology, #2118), and anti-HSP90 (Cell Signaling Technology, #4874) were validated by their respective manufacturers, with detailed characterization available on their official websites.

Eukaryotic cell lines

Policy information about cell lines and Sex and Gender in Research

Cell line source(s): HEK293T cells were used in this study, which were obtained from the American Type Culture Collection (ATCC).

Authentication: Identity of the cell lines was frequently checked by their morphological features but have not been authenticated by the short tandem repeat (STR) profiling.

Mycoplasma contamination: The HEK293T cell line was tested to be mycoplasma-negative by the standard PCR method.

Commonly misidentified lines (See ICLAC register): No commonly misidentified cell lines are used in this study.

Palaeontology and Archaeology

Specimen provenance: *Provide provenance information for specimens and describe permits that were obtained for the work (including the name of the issuing authority, the date of issue, and any identifying information). Permits should encompass collection and, where applicable, export.*

Specimen deposition: *Indicate where the specimens have been deposited to permit free access by other researchers.*

Dating methods: *If new dates are provided, describe how they were obtained (e.g. collection, storage, sample pretreatment and measurement), where they were obtained (i.e. lab name), the calibration program and the protocol for quality assurance OR state that no new dates are provided.*

☐ Tick this box to confirm that the raw and calibrated dates are available in the paper or in Supplementary Information.

Ethics oversight: *Identify the organization(s) that approved or provided guidance on the study protocol, OR state that no ethical approval or guidance was required and explain why not.*

Note that full information on the approval of the study protocol must also be provided in the manuscript.

Animals and other research organisms

Policy information about studies involving animals; ARRIVE guidelines recommended for reporting animal research, and Sex and Gender in Research

Laboratory animals	The study utilized wild-type (WT) C57BL/6J mice, ADORA1-/- mice (NM-KO-225140, Shanghai Model Organisms Center, Inc.), ADORA2A-/- mice (NM-KO-200018, Shanghai Model Organisms Center, Inc.), CD73-/- mice (provided by Dr. Jiangfan Chen, Wenzhou Medical University) and Rosa26-Cas9-GFP mice (Gt (ROSA)26Sortm1.1(CAG-cas9*, -EGFP) Fezh/J; the Jackson Laboratory, cat. no. 024858). All animal procedures were performed in accordance with protocols approved by the Institutional Animal Care and Use Committee (IACUC) of the Chinese Institute for Brain Research, Beijing (CIBR), and complied with the national guidelines for the housing and care of laboratory animals set by the Ministry of Health, China. Mice were housed in a specific pathogen-free (SPF) facility on a 12-h light/dark cycle with ad libitum access to food and water. The SPF facility temperature was set to ~20.5-22.5 °C and humidity to ~45-65%. All experiments were conducted on male and female mice aged 8–16 weeks.
Wild animals	No wild animals are used in the study.
Reporting on sex	Both female and male mice are used in the experiments and data are plotted without discriminating the sex.
Field-collected samples	This study did not involve samples collected from the field.
Ethics oversight	All animal surgery and experimentation procedures are performed according to protocols approved by the Animal Care & Use Committees of Chinese Institute for Brain Research (#CIBR-IACUC 001).

Note that full information on the approval of the study protocol must also be provided in the manuscript.

Clinical data

Policy information about clinical studies

All manuscripts should comply with the ICMJE guidelines for publication of clinical research and a completed CONSORT checklist must be included with all submissions.

Clinical trial registration	*Provide the trial registration number from ClinicalTrials.gov or an equivalent agency.*
Study protocol	*Note where the full trial protocol can be accessed OR if not available, explain why.*
Data collection	*Describe the settings and locales of data collection, noting the time periods of recruitment and data collection.*
Outcomes	*Describe how you pre-defined primary and secondary outcome measures and how you assessed these measures.*

Dual use research of concern

Policy information about dual use research of concern

Hazards

Could the accidental, deliberate or reckless misuse of agents or technologies generated in the work, or the application of information presented in the manuscript, pose a threat to:

No	Yes	
☐	☐	Public health
☐	☐	National security
☐	☐	Crops and/or livestock
☐	☐	Ecosystems
☐	☐	Any other significant area

Experiments of concern

Does the work involve any of these experiments of concern:

No	Yes	
☐	☐	Demonstrate how to render a vaccine ineffective
☐	☐	Confer resistance to therapeutically useful antibiotics or antiviral agents
☐	☐	Enhance the virulence of a pathogen or render a nonpathogen virulent
☐	☐	Increase transmissibility of a pathogen
☐	☐	Alter the host range of a pathogen
☐	☐	Enable evasion of diagnostic/detection modalities
☐	☐	Enable the weaponization of a biological agent or toxin
☐	☐	Any other potentially harmful combination of experiments and agents

Plants

Seed stocks

Report on the source of all seed stocks or other plant material used. If applicable, state the seed stock centre and catalogue number. If plant specimens were collected from the field, describe the collection location, date and sampling procedures.

Novel plant genotypes

Describe the methods by which all novel plant genotypes were produced. This includes those generated by transgenic approaches, gene editing, chemical/radiation-based mutagenesis and hybridization. For transgenic lines, describe the transformation method, the number of independent lines analyzed and the generation upon which experiments were performed. For gene-edited lines, describe the editor used, the endogenous sequence targeted for editing, the targeting guide RNA sequence (if applicable) and how the editor was applied.

Authentication

Describe any authentication procedures for each seed stock used or novel genotype generated. Describe any experiments used to assess the effect of a mutation and, where applicable, how potential secondary effects (e.g. second site T-DNA insertions, mosiacism, off-target gene editing) were examined.

ChIP-seq

Data deposition

☐ Confirm that both raw and final processed data have been deposited in a public database such as GEO.

☐ Confirm that you have deposited or provided access to graph files (e.g. BED files) for the called peaks.

Data access links
May remain private before publication.

For "Initial submission" or "Revised version" documents, provide reviewer access links. For your "Final submission" document, provide a link to the deposited data.

Files in database submission

Provide a list of all files available in the database submission.

Genome browser session
(e.g. UCSC)

Provide a link to an anonymized genome browser session for "Initial submission" and "Revised version" documents only, to enable peer review. Write "no longer applicable" for "Final submission" documents.

Methodology

Replicates

Describe the experimental replicates, specifying number, type and replicate agreement.

Sequencing depth

Describe the sequencing depth for each experiment, providing the total number of reads, uniquely mapped reads, length of reads and whether they were paired- or single-end.

Antibodies

Describe the antibodies used for the ChIP-seq experiments; as applicable, provide supplier name, catalog number, clone name, and lot number.

Peak calling parameters

Specify the command line program and parameters used for read mapping and peak calling, including the ChIP, control and index files used.

Data quality

Describe the methods used to ensure data quality in full detail, including how many peaks are at FDR 5% and above 5-fold enrichment.

Software

Describe the software used to collect and analyze the ChIP-seq data. For custom code that has been deposited into a community repository, provide accession details.

Flow Cytometry

Plots

Confirm that:

☐ The axis labels state the marker and fluorochrome used (e.g. CD4-FITC).

☐ The axis scales are clearly visible. Include numbers along axes only for bottom left plot of group (a 'group' is an analysis of identical markers).

☐ All plots are contour plots with outliers or pseudocolor plots.

☐ A numerical value for number of cells or percentage (with statistics) is provided.

Methodology

Sample preparation	*Describe the sample preparation, detailing the biological source of the cells and any tissue processing steps used.*
Instrument	*Identify the instrument used for data collection, specifying make and model number.*
Software	*Describe the software used to collect and analyze the flow cytometry data. For custom code that has been deposited into a community repository, provide accession details.*
Cell population abundance	*Describe the abundance of the relevant cell populations within post-sort fractions, providing details on the purity of the samples and how it was determined.*
Gating strategy	*Describe the gating strategy used for all relevant experiments, specifying the preliminary FSC/SSC gates of the starting cell population, indicating where boundaries between "positive" and "negative" staining cell populations are defined.*

☐ Tick this box to confirm that a figure exemplifying the gating strategy is provided in the Supplementary Information.

Magnetic resonance imaging

Experimental design

Design type	*Indicate task or resting state; event-related or block design.*
Design specifications	*Specify the number of blocks, trials or experimental units per session and/or subject, and specify the length of each trial or block (if trials are blocked) and interval between trials.*
Behavioral performance measures	*State number and/or type of variables recorded (e.g. correct button press, response time) and what statistics were used to establish that the subjects were performing the task as expected (e.g. mean, range, and/or standard deviation across subjects).*

Acquisition

Imaging type(s)	*Specify: functional, structural, diffusion, perfusion.*
Field strength	*Specify in Tesla*
Sequence & imaging parameters	*Specify the pulse sequence type (gradient echo, spin echo, etc.), imaging type (EPI, spiral, etc.), field of view, matrix size, slice thickness, orientation and TE/TR/flip angle.*
Area of acquisition	*State whether a whole brain scan was used OR define the area of acquisition, describing how the region was determined.*

Diffusion MRI ☐ Used ☐ Not used

Preprocessing

Preprocessing software	*Provide detail on software version and revision number and on specific parameters (model/functions, brain extraction, segmentation, smoothing kernel size, etc.).*
Normalization	*If data were normalized/standardized, describe the approach(es): specify linear or non-linear and define image types used for transformation OR indicate that data were not normalized and explain rationale for lack of normalization.*
Normalization template	*Describe the template used for normalization/transformation, specifying subject space or group standardized space (e.g. original Talairach, MNI305, ICBM152) OR indicate that the data were not normalized.*
Noise and artifact removal	*Describe your procedure(s) for artifact and structured noise removal, specifying motion parameters, tissue signals and physiological signals (heart rate, respiration).*

Volume censoring

Define your software and/or method and criteria for volume censoring, and state the extent of such censoring.

Statistical modeling & inference

Model type and settings

Specify type (mass univariate, multivariate, RSA, predictive, etc.) and describe essential details of the model at the first and second levels (e.g. fixed, random or mixed effects; drift or auto-correlation).

Effect(s) tested

Define precise effect in terms of the task or stimulus conditions instead of psychological concepts and indicate whether ANOVA or factorial designs were used.

Specify type of analysis: ☐ Whole brain ☐ ROI-based ☐ Both

Statistic type for inference

Specify voxel-wise or cluster-wise and report all relevant parameters for cluster-wise methods.

(See Eklund et al. 2016)

Correction

Describe the type of correction and how it is obtained for multiple comparisons (e.g. FWE, FDR, permutation or Monte Carlo).

Models & analysis

n/a	Involved in the study
☐	☐ Functional and/or effective connectivity
☐	☐ Graph analysis
☐	☐ Multivariate modeling or predictive analysis

Functional and/or effective connectivity

Report the measures of dependence used and the model details (e.g. Pearson correlation, partial correlation, mutual information).

Graph analysis

Report the dependent variable and connectivity measure, specifying weighted graph or binarized graph, subject- or group-level, and the global and/or node summaries used (e.g. clustering coefficient, efficiency, etc.).

Multivariate modeling and predictive analysis

Specify independent variables, features extraction and dimension reduction, model, training and evaluation metrics.